Rebuttal letter

Title: Atmospheric polarimetric effects on GNSS Radio Occultations: the ROHP-PAZ field campaign

Authors: R. Padullés, E. Cardellach, M. de la Torre Juárez, S. Tomás, F.J. Turk, S. Oliveras, C. O. Ao, and A. Rius

Doi: 10.5194/acpd-15-18747-2015

First of all, we would like to thank the reviewers for their time and effort to review our manuscript. We acknowledge the comments, concerns and suggestions, that we have addressed and we believe that resulted in and improved manuscript.

All the changes made are explicitly shown in a *"latexdiff"* style document provided at the end of this letter. All the comments made by the reviewers are addressed individually in the following text, and some major changes have been done: we have added a sub-section in Sec. 2; and some paragraphs of Sec. 5.2 have been rewritten.

Reviewer #1:

This is a very interesting and important paper that demonstrated the polarimetric signatures introduced by the hydrometeors with in the GNSS radio occultation (RO) signals can be measured through a ground-based GNSS receiver equipped with two polarimetric antennas. This is a follow-up demonstration of the proof of concept proposed in a theoretical simulation study by Cardellach et al. (2015), which shows the differential phase between the horizontal and vertical polarimetric components is introduced by the hydrometeors along the radio link. The paper provided an important step-stone for the upcoming Spanish PAZ satellite mission that is targeting to provide the heavy precipitation detection capability with polaritric GNSS measurements.

The low elevation angle GNSS measurement (0-20 deg) covering various meteorological conditions (no rain, wet and rain days) during a 8-month field campaign on mountain peak at 1670 m above MSL. Near-coincident Meteorological C-band radar observation were interpolated into with the GNSS RO signal ray trajectory to identify and quantify the rain rate. Case studies were used to demonstrate the capture of the polaritimetric signatures induced by the hydrometeors along the radio-link based on the time series of the RO measurements, which is validated with the near coincident radar and ground station measurements. A forward scattering simulation was also carried out to explain the polarimetric GNSS observation. The data analysis shows that other than the rain droplet, the hydrometeors such as melting particles and ice crystals could have significant impact on the polarimetric phase difference measurements.

Overall the paper has important contribution to advance the understanding the hydrometeors impact on the RO polarimetric signals. It also provided the observational evidence for the upcoming PAZ satellite mission, which will use spaceborne GNSS RO for heavy precipitation measurements. However, the presentation of the work need some significant improvement. I would recommend the publication of the article after addressing the following issues:

Major comments:

1. The authors write the most part of the paper in the "first person", which would be better to be in the "third person". Some very short paragraphs (only one or two sentences) that should not be stand alone. The authors tend to use the "symbols" on discussion, which could cause big challenges for readers. Better to use the real observables (e.g., rain rate, instead of R especially when it does not shown up repeatedly)

Following the reviewer advices, we have made changes to the text to make it easier for the reader to follow. We have also corrected the length of some paragraphs. Regarding the use of the first / third person, we have changed the possessive expressions, such as "our data", "our receiver", etc., by impersonal expressions like "the data", "the receiver", etc. However, we have kept the first person when we are referring to procedures or obtained results, (like in "We performed", "we derived", …). There is some controversy in this matter, but we believe that if we are consistent all along the manuscript, first person expressions are better than passive ones. We have found arguments in favor and against in the following website: *https://cgi.duke.edu/web/sciwriting/index.php?action=passive_voice* .

2. Section 2.2, the process to derive the multipath is not clearly presented. More details are needed.

We have rewritten section 2.2, and we believe that now all the process is clearer. We have also added a new sub-section to separate in a better way the contributions to the signal in addition to the local multipath, and now the section is more complete.

3. The Nowcasting and Very Short Range Forecasting (NWC-SAF) data description need some more details, such as horizontal resolution, what satellites in what band. Sounds like the data were not very critical in this research (only shown up in Fig. 4). If so, the dataset could be removed from the paper.

We have written an extra paragraph giving more details about the NWC-SAF data and a reference has been added. These data are used in the research to identify ice contribution above the radar measurements (section 5.2). It has also been clarified and we have kept everything related to this dataset.

4. Many Figures require improvements before publication, such as Figure 1, 8, 9, 11 and 12. More specific comments are in the next section.
a. Figure 1, better to mark/name the locations of the GPS antenna, weather radar and the near-by ground stations if included.
b. Figure 9 is hard to read. Prefer with larger font.
c. Figure 11 and 12 need to be improved. Hard to read. Suggest to remove the un-necessary x or y axis caption and enlarge the figures.

We have changed Figure 1 in order to show the antenna's main lobe and the tracks of the satellites. The required changes in Figures 9, 11 and 12 have been also performed.

5. Section 5.3 is one of the most important section but the main text is a mess and require significant cleanup.
P18764: The main text need to discuss/summarize the results on the Figure 10. You can't simply state "Fig. 10 is a illustrative case..."

We have added a description of the Fig 10, 11 and 12 in the main text, in Sec. 5.3

P18783-4: Figure 10 is confusing. The "orange shaded area" should be only ONE-color based on the simulation, right? Is the color variation inside the orange boxes due to the radar reflectivity? If so, the orange boxes shouldn't use shade, but simply a transparent box with color outline, without blocking the radar reflectivity contours. Same comments apply to Figure 11 and 12.
We have improved the Figures by changing the orange shaded area by a transparent one, delimited by a dashed

line. We believe that now is easier to interpret.

6. P18754-L1-3: Provide the "threshold" number of the radar reflectivity (Ze) for "rain-days" instead of using the vague "significant reflectivity". Does the same radar reflectivity threshold used to define no-rain days. Also, is there a requirement for how long the "rain" lasts to be counted as "rain-days"?
"We define as no-rain days those days when no rain is present in the area ..." -> The radar reflectivity factors (Ze) are used to identify the "rain-days", with Ze exceed ### ....

P18757: Similarly, in Section 4.2, the criteria for separating the three meteorological conditions is confusing and better to be more quantitatively. Also the three "σ" should be removed, which can be listed in L3. "The standard deviation of the differential phase delay as a function of elevation for different meteorological conditions, such as σ_dry, σ_wet and σ_rain are computed:"

The identification of *rain / wet / no rain* days depends on two factors: the ground weather stations and the reflectivity factor from the weather radar. Depending on the nearby ground weather station accumulated rain during the observation time and whether the interpolation of the GNSS rays with the weather radar had crossed an area with any valid values of Ze or not, the days are labeled as *rain, wet* and *no rain*. This has been explained in sections 2.2, 3, and 4.

L9: "with rain in the surroundings", any "number" used to define the area, such as within 50 km or 100km radius of the GNSS station?

When we referred to the surroundings we meant the area crossed by the GNSS rays. We have changed the definitions in section 4.1 to make it more clear.

7. P18761-L15: The key results such as the correlation between the observed and simulated AΦ (improvement from 0.6 to 0.75) shouldn't only be mentioned in the Figure-8 caption (P18781). The result need to be summarized in the main text too.

We want to clarify the ideas regarding Figure 8:

- The correlation coefficient improves when including all the hydrometeors
- The ancillary improvement, from 0.6 to 0.75 (caption of Fig. 8) occurred when less points, of lower signature, were taken into account.
- In any case, these correlation numbers are not significant, as we could not simulate the actual meteorological conditions of each simulated event.

Because these points above, we have now removed the correlation coefficient numbers from the article.
What we consider significant is the slope of the fitted line (dot-dashed in Fig. 8). We find:

- All hydrometeors fit's slope is much closer to 1 than only rain fit's one. This indicates that inclusion of icy and melting particles explains the polarimetric singature at the right order of magnitude.
- Moreover, the all-hydrometeors fitted line (below 1) corresponds to simulation with an overestimated polarimetric effect. Indeed, because we do not know, for instance, the exact percentage of oriented ice particles, we have assumed a 100% (which is likely to be an overestimation).

The text now explains this rationale.

8. P18764-L9: Again, Figure 10 need to be explained in the main text. The context should not be only mentioned in the figure caption.

An explanation in section 5.3 has been included.

9. P18763-L3: The correlation between the observed and simulated AΦ seemed to increase from 0.6 to 0.75 after including the ice & mixing phase particles. Should the adding criteria of "AΦ < 20 mm · deg" be "AΦ > 20 mm · deg" (in P18781) instead that lead to increasing correlation?
All this results need to be included in the main text. Also it is probably more informative to highlight those "dots" that satisfy the extra criteria on Figure 8.
However, Figure 8 still shows rather large scattering. Any other explanation?

Please see our answer to point 7 above.

10. P18762-L20: What is the typical time/distance difference between the METEOCAT's radiosondes to the major part of precipitation? Is the radiosonde temperature profile representative enough to guiding the phases of the particles?

The antenna is pointing south, where the radiosondes are launched (Barcelona city). The distance is less than 50 km, and the time difference between the launch of the radiosonde and the events can be of several hours (the radiosondes are launched twice per day, at 12 and 00 UTC). However, temperatures above the boundary layer (~ 2 km) should be representative enough.

Radiosonde measurements are the closest to a true value that is available in the area. We do not consider that the possible error in temperatures is worse than the possible error done in the interpolation of the rest of the weather data, and we believe that it is enough for the scope of this work.

Any direct evidence of the "ice" particle presence from the near-coincident radar measurements that support the IWC amount (e.g., 1gm-3) etc. in the simulation?

We have added a reference with measured values around 1 gm-3, from the retrievals of Cloudsat, Calipso and Modis. Unfortunately, no collocations with these three satellites were found.

Other minor comments:

11. P18749-L21: "These GNSS satellites are identified by ..."
Corrected.

12. P18752-L8: "denotes"
Corrected.

13. P18752-L9: What is "hardware effects" means? Is that "receiver measurement noise"?
We have added some examples of hardware effects.
L10: Replace "K" in eq-3 with another character, as it could be confused with the "Kdp", the specific differential phase in eq. 1
We changed "K" by "b".

14. P18754-L11: Brief explain how the antenna pattern looks like and why it affects the multipath pattern. Reference is needed, i.e., Cardellach et al., 2015.
A brief explanation about the antenna pattern and a reference to Cardellach et al., 2015 has been added into the new section 2.4, that describes the effects that are affecting the precision of the measurement and cannot be directly corrected, but have to be characterized inside the multipaht "m" term.

15. P18755-L5: "We have been provided by the data from ..." -> The weather radar, in-situ radiosonde and the METEOSAT satellite measurements near the GNSS observational site are used in this study.

L17: has also -> also has
In a radius of 30km around the GNSS site, there are 5 ground weather stations, with one locating a few meters from the GNSS antennas.
Corrected. We really appreciate the corrections and suggestions.

L23: remove “the Support to”
Done.

L24: NWC-SAF: need more information regarding the model product, such as horizontal resolution, what satellite observations are assimilated? How accurate is the CTH especially during the rain? Reference need to be cited.
We have provided a reference and more information about the NWC-SAF products. Regarding the accuracy of CTH during rain, we have not noticed any significant difference in the data quality among days that correlate with rain. Also, NWC-SAF is also obtaining precipitation products from these physical properties products (such as cloud top height, cloud top phase, and the ones resulting from these).

L25: “These data results...” -> These data product is a combination of satellite observation and Numberical weather Prediction (NWP) model simulations.
Corrected.

16. P18756-L1: What satellite imagery? Visible band? Are the infrared and microwave observations included?
Answered in points 3 and 15.

L3: Rewrite “Using the CTY and CP ... of the top of the cloud. Combining this information ...” -> The cloud observation from NWC-SAF (CTY, CP and CTH) are then collocated with the GNSS ray trajectories.
Done. Thanks to the reviewer for the suggestions.

L11: “Even though the temporal resolution is not very high” -> “With the limited two-time daily soundings, the temperature and refractivity profiles can be interpolated into the GNSS observation time.
Done.

L15: “collocation of the observations” -> “collocations of the GNSS polarimetric observations”
Done.

L24: “Standard deviation” -> would be better to be more informative, such as “Polarimetric signature”
We have changed the title “Standard deviation” by “Polarimetric signatures in \Delta \Phi standard deviation”, and we agree with the referee that it is more informative.

17. P18757-L1: “standard deviation” of ??
L2: in three sub-sets -> into three meteorological condition. Suggest to replace“subset” with “met”.
We have followed the suggestion of the referee and we have changed the “subsets” by “meteorological conditions”.

L11: “environmental situation” -> “meteorological conditions”
Done.

L14: “the results of ... and for the three day sub-sets” -> “the mean σ across all elevation observations for each GNSS satellite during the three different meteorological conditions are summarized in Table 2.”
Changed.

L21: The larger σ in rain-days comparing with the wet-days indicates other factor(s) should have contributed to

the enhanced polarimetric signature other than the enhanced multipath due to the wet soil in the rain-days.

Better to state clearly, the wet-days and rain-days both could have wet soil condition, which could lead to enhanced multipath and so larger σ.

Would be good to also comments that such mulitipath will not be an important factor for spaceborne case.

We have followed the suggestions of the referee and we have changed the text to better state the point that the enhanced multipath should come from other sources than wet soil. Also, comments about the multipath differences between the spaceborne and the field campaign scenarios are stated in Table 2.

L24: How to compute multipath_no-rain?
Clarified in the last paragraph of section 4.1.

18. P18758-L22: This is one of the most important conclusion from the paper and could be better written. "This represents...signals." -> "This is the first direct observational evidence of the polarimetric signatures induced by the precipitation in the GNSS signals."
We have rewritten the mentioned text.

19. P18759-L1: How about making the section title more informative such as, "Model study on the hydrometeors on the GNSS polarimetric signals"
We have kept the title as it was originally written, since we think that is better to keep the question style in concordance with section 4 title.

L11: what is the "R" on the denominator?
The R is actually the Real part symbol. It is written in Latex, and we have left it as it is, hoping that in the final version the font type will be more clear. If this is not the case, we will ask for a change.

20. P18760-L1: "Kw=(mw2 -1)..." in the eq. 12?
Corrected.

L4: "The reason is that ..." -> This will allow to relate the reflectivity from the weather radar in C-band with the GNSS observations in L band.
Changed

L11: what the meaning of "through its moments"?
We have removed the "moments" mention, since can lead to an unnecessary confusion and the text meaning is be entirely kept.

21. P18761-L6: "because the ... suggested so" → as suggested by the meteorological ground stations
Corrected.
L7: "and we have limited ..." -> and an upper limit of LWC is set to be 3 gm-3 according to the observational evidence of severe storms described in Black andHallett(2012).
Changed.

L19: polarimetric signals observed (black dots in Fig. 8)
We have included the suggested mention in the text.

22. P18762-L23: How representative is the radiosonde sounding for such a large area of the radar observation. Would it be a problem of using the radiosonde many km away to represent the temperature of a storm?

As we have said in comment #10, the radiosonde data should be representative enough above the boundary layer, where most of our analysis happen. In the case of a storm, it is true that if the rain cell is very small, the temperature obtained by the radiosonde may not be correct. Yet, these measurements are the closest to a true value that is available in the area.
However, thermodynamics inside storms is still an open problem, and one of the aims of the ROHP-PAZ mission is to improve it.

23. P18763-L11: The discussion on the model uncertainty is not well presented. The tone of the writing made a bad impression to the readers that the model might be too simple and could be "wrong". Would be more persuasive by focusing on what the simple model is capable of doing, e.g., explain the major portion of the observations. In the mean time, discuss the potential impact of such "unsimulated" factors on the simulation results.
We have changed some parts of this paragraph to avoid negative tone in the expressions.

L23: Remove: "The goal of ... signatures". No need to say the goals, but focus on the results.
Removed

L26: "other hydrometeors" -> icy and mixing-phase particles significantly increases …
Corrected

L27: "why favoured higher Kdp?
Explained in the text, which has been changed with respect the original one.

24. P18764-L11: Very messy section in writing, need some significant improvement.
L16: "It can be seen..." -> Large positive $\Delta\Phi$ is present when large radar reflectivity (Ze)
Changed.

L27: "more than 90%", where is this number coming from? Better to state # of cases that is consistent with the model simulation. Also what is the criteria of "consistent cases"?
The # of cases has been given, and also the number of those that can be explained by the model simulation and what is cosidered consistent is explained.

25. P18765-L2: "reflectivity" -> radar reflectivity.
Changed.

L3: Can the discrepancy in G15 due to the missing observational in radar? Or the false alarm in the hydrometeors in the model, which relies on the radiosonde temperature profiles that might not be representative inside the storm.
This could be an hypothesis. We have added this possible explanation at the end of section 5.3.

L7: "with the aim of..." -> and the evidence of the polarimetric signature induced by the hydrometeors in the GNSS signals has been presented.
Corrected.

Some "passive words" were used in this session, which generated unnecessary negative impression on the research work and better to be changed. For example:
L19 "out of our control"
L20 "None of these effects are expected (or not as severely)"...
P18767-L2 "but we feel that this would be too speculative and impossible to validate..."
We have made some changes in these expressions that removed the negative impression.

26. P18772: “Measurement difference between the ROHP-PAZ spacebore ...” Could simply add one more column for “parameters”, for initial phase delay, local multipath and Thermodynamic profile” to reduce the redundancy.
We have added an extra column indicating the parameter. Now the Table looks better.

27. P18773: The standard-deviation of the polarimetric phase differences under three meteorological conditions (e.g, dry, wet and rain days). “for each day set i" -> for each meteorological condition.
Changes made in the caption.

28. P18777: “Illustration .... Ray trajectory” -> A vertical slice of radar reflectivity (shaded) at two epoch of a rising GNSS occultation event.
Remove “collocated with the CP...trajectory”
Changes done.

29. P18779: Figure 6, “Target shapes used” -> Particle shape models used
“Oblabe ellipsoid, used to reproduce rain” -> Oblate ellipsoid for rain drops, (middle) two concentric ellipsoids for melting ice particles, ... (right) Dendritic shape for pristine ice particles.
Changed.

30. P18780: typo: “hydrometeor”
Corrected.

31. P18781: Figure 8. Better to use two square panel. Remove “the gray dashed ... modelling”
Should “it decreases to r=0.75” to be “increase to”?
20mm.deg -> 20 mm • deg, where are those dots in the plot???
We have changed the figure to use a two square panel. We have also changed the caption, which was confusing and we removed the “r” concept. Now we only refer to the fitted lines, no mention to r coefficient.

32. P18779: Figure 10, X-caption: Reflectivity “Z” -> “Ze”.
Done

33. P18784: Figure 11: Why the time of the bottom two panels (left and right columns) are flipped. Remove the unnecessary X/Y axises caption to allow larger plot for each individual panels. Increase font size.
G022 should be G22 at the 2nd panel on the left column
The time was taken at the beginning of the observation, and in this case the observation of G22 was much longer than G31 (it started at a high elevations, while G31 started close to 20 deg). We changed the time acquisition method to make it more representative of the event plotted: the time that is annotated now in each panel corresponds to when the elevation is 10 deg.

34. P18785: Figure 12: suggest use two column plot with 3 panel in each column. Also add time for the first panel (“no data”).
“with the used hydrometeors” -> by the model simulation. The discrepancy might not necessary be only due to the problem of the hydrometeors used in the model, but attributed to the radar observation or other factors in the model simulation.
We keep the panels in a vertical format, to make it easy to compare with Figure 11. The time and the caption has been modified.

Reviewer #2:

This paper describes an experiment done in preparation for a satellite mission that itself is a proof-of-concept for detecting precipitation using GNSS limb sounding. The observation principle is that water and other atmospheric meteors induce a polarization on GNSS signals traversing the atmosphere. With polarization-sensitive antennas, it is expected that precipitation events in the GNSS ray-path should be detectible in GNSS radio occultation geometry, GNSS RO being a new yet significantly advanced field in remote sensing of the atmosphere. The space mission will be PAZ; this paper is a field campaign with a GPS receiver placed on a mountaintop to investigate the viability of the method in situ before PAZ is deployed. The mountaintop receiver tracked 5 GPS satellites over the course of the course of approximately a half year in 2014. Significant signal processing was undertaken to eliminate the effects of ill-determined total phase and local multipath in signal propagation to the best of the authors' capability. After "correcting" the data, limb soundings whose differential phase—representing the difference in phase between horizontal and vertical polarizations—are outliers, are considered as influenced by precipitation. Simulations of differential phase based on water meteors underestimate the observed differential phase for these soundings. Simulations of differential phase with ice and snow in addition to water meteors are more consistent with observations than simulations with water meteors only.

The manuscript is in need of major clarification and possibly a large effort in revised data analysis. While there may or may not be enough detail presented to recreate the data analysis, the manuscript is lacking in justification for some of the steps taken. Moreover, the authors possibly commit a serious error in their interpretation of their statistical analysis.

- Paragraph, lines 10–23 of p.18749: The authors state that only 5 GPS satellites fall within the occultation antenna pattern. Why does this come about? How many times daily for each satellite? Are these both rising and setting satellite trajectories, or just setting trajectories? What do the trajectories for each GPS satellite look like in elevation-azimuth coordinates? Where are the multipath sources in this space?

We have chosen the 5 best GPS satellites in terms of signal strength, number of tracked days and presence of both days free of rain and days with rain. The receiver used in this experiment was also connected to an hemispherical antenna pointing to the zenith. The receiver, according to internal algorithms out of our control and the visible satellites from the "zenith-pointing" antenna, was tracking a number of satellites that was not the same every day. Thus, only those GPS that crossed the main beam of the polarimetric antenna (which pointed south and to the horizon) and were tracked most of the days, were chosen.
These satellites have a sidereal orbit, thus they repeat its trajectory in the sky (as seen from the observation site) sidereal day after a sidereal day. This implies that when tracked, a GPS is in the same position regardless of the date. The best suited and with better signal are those placed in the azimuth corresponding to the boresight of the antenna (where the antenna is pointing at), and in a position that is free of obstacles like antennas, fences, metallic structures, etc. (see figure 1 for an example of these structures). In summary, we have chosen those for which we have enough days with good tracking and the best signal strength in comparison with all the available data. We understand as signal strength, the measure of SNR that is received.

The chosen satellites follow trajectories that have an azimuth varying between very few and ~20 degrees, and elevation varying from 0º to 20º-40º. We only use the information of the segment that fall inside the 0-20º range of elevation, although the satellite is tracked whenever is visible to the polarimetric antenna. We have added in the article text (Sect. 1) that the polarimetric antenna was pointing south and to the horizon, which was not mentioned and could lead to misunderstandings. Again, this range is chosen to take the best signal strength and also because is the closer situation to a Radio Occultation geometry. Both setting and rising trajectories are used, and some of the chosen satellites are seen twice a day. Some satellites can be seen twice per day (depending on their orbit inclination), but sometimes one of these trajectories could fall in the opposite azimuth with respect the other, and generally this implies that one of them will be difficult to track.

- Equation 1: In the presence of "bi-refraction" (my term), do the GPS rays follow the same path through the atmosphere? Would path separation lead to an amplification or diminution of phase differential?

The emitted wave at the GPS satellite is a Right Handed Circular Polarized (RHCP). Generally, it is also received at this polarization, thus wave components have had to follow the same path through the atmosphere, otherwise the RHCP receiver would not be able to reconstruct the signal. In this experiment, what we are trying to see is a very small effect of "bi-refraction" caused by hydrometeors (few mm, with respect the thousands of km that the signal is travelling), that induce a different effective propagation constant to the vertical and the horizontal components and it might lead to slightly more elliptical polarization state. Receiving the wave in a double polarization antenna (H – V) allows us to see this small effect in the phase delay (or slightly different path) between both components. A mention to bi-refraction has been included in Section 1. At this moment we are not aware of other atmospheric phenomena acting as source of depolarization. Exhaustive analysis of PAZ data will help us investigating this hypothesis.

- Line 25ff, p.18751: Where does the "initial measurement" take place? It was previously stated that tracking took place between 0º and 20º elevation. (Hopefully the receiver actually tracked into negative elevations.) How long are the tracking arcs typically? Shouldn't it be possible to get a pseudo-range without L2 inasmuch as the receiver was able to track L1/CA and the ionospheric influence is very much the same for both polarizations as argued in section 2.3? I can imagine many methods one might use to establish $K^H - K^V$ absolutely and not have to subtract a profile mean $\Delta\Phi$.

The "initial measurement" depends on every single tracking. Is is referred either to when the tracking of a satellite starts, or to when the tracking is broken and it starts again. Every time that the tracking starts, the first phase measurement is an arbitrary and unknown value, and the following measurements are relative to it.
This initial measurement does not need to be inside the 0-20 degrees of elevation. We use the measurements inside this range because it is where the antenna performs better (due to its orientation pointing south and to the horizon), although satellite visibility reaches higher elevations (~40 deg). Not many negative elevation measurements are available. However, negative elevations would be useful if we wanted to retrieve the standard thermodynamic products, such as refractivity profiles, which was not our aim in this experiment.
The length of the tracked arcs is variable. Most of them last between 20º and 5º of elevation without being broken. The continuity of the arcs is more likely to be broken when the elevation is low, since the signal is crossing more atmospheric layers as the elevation decreases, and it can be weakened or bended too much by an extra refractive area more easily.
Regarding the phase ambiguity resolution, we have tried the following method using pseudorranges:

Being P and L the pseudo-range and the carrier phase observables, we computed the difference between the two polarizations of each of them:

$\Delta L_{H\text{-}V}(t) = \Delta\, \rho^r(t) + \Delta C(t)$

$\Delta P_{H\text{-}V}(t) = \Delta\, \rho^r(t) + \Delta B(t) + \Delta b$

where $\Delta\, \rho^r(t)$ is the rain contribution, $\Delta C(t)$ and $\Delta B(t)$ are hardware errors and Δb is the initial phase difference. Here it has been assumed that the ionospheric delay is the same in both polarizations.
Since $\Delta C(t)$ and $\Delta B(t)$ are small, we can consider that:

$$\widehat{\Delta b'} = \langle \Delta L(t) - \Delta P(t) \rangle$$

where $\Delta C(t)$ and $\Delta B(t)$ have been absorbed in the measured quantities as errors.

Using this procedure we are able to correct the phase ambiguity with a precision of several centimeters. However, this precision is not enough to solve what we are looking for. We need precisions of the order of mm to be able to measure the phase delays caused by hydrometeors.

We have removed the term L2 after Eq. 3 because, in fact, we tried with both L1 and L2.
We are open to suggestions on how to obtain the phase ambiguity with enough precision.

- p.18753: Twice the term "homogenize" is used to describe to different steps in data processing. What does this term mean? If a data segment is "homogenized" once, why must it be "homogenized" a second time? The authors should decide whether to spell the term "homogenize" (l.1) or "homogenise" (l.24).

We have removed the second "homogenise" term, since it was not necessary. With this term we wanted to refer to a step that allows comparison among different days.

- Section 2.2: The authors use the term "multipath" where the radio occultation community customarily uses the term "local multipath". Isn't it possible that the atmospheric boundary layer also induces multipath? That would be "atmospheric" multipath.

We agree with the referee that "multipath" should be referred to as "local multipath". We have performed the appropriate changes in the text. With respect to the atmospheric multipath, it is due to complex refractive structures that yield several possible optical paths. We believe that it does not induce polarimetric features (i.e. different features in H and V components), unlike local multipath, which is partially due to linear elements (metallic edges, bars, columns, ...) that induce different features in the different polarizations.

- Line 27, p.18753: The average of all arcs for each GPS satellite respectively can be expected to give the observational response to the mean environmental conditions. The authors have made differential phase a function of satellite elevation but not of satellite azimuth. Do all the trajectories for a given satellite follow the same elevation-azimuth track? If not, then a component of the standard deviation is due to changes in geometry (different azimuth track). Otherwise, the standard deviation represents the dynamic range of the observations due to changes in environmental conditions and is not error in the multipath signal, which is implied in the manuscript. Error in the multipath signal is better described by the standard error, or the standard deviation divided by the square-root of the number of arcs considered in the mean.

All the satellites follow the same elevation-azimuth track, with a sidereal period.
When we have computed the standard deviation in the manuscript, we were always referring to the dynamic range of the observations, not to the error of the multipath signal. For example in Fig. 3, what we plot is the multipath pattern m and its dynamic range, so a shaded area between $m + \sigma$ and $m - \sigma$ (in blue) and $m + 2\sigma$ and $m - 2\sigma$ (in gray). We have made some corrections in the text to state it more clearly.

- Lines 25-26, p.18754: Offer some support for this statement.

A more extensive explanation about the ionospheric effects has been included in section 2.3.

- Line 5, p.18756: What does it mean to "properly collocate our observations"?

We have changed this expression. We have made clear that the collocated weather observations are interpolated with the GNSS rays.

- Lines 1-6, p.18758: It is not clear in the text what the standard deviation is. I infer that it is the root-mean-square of the "corrected" phase differential by satellite $\Delta\Phi_{day}{}^{PRN}(\varepsilon)$ for non-moist conditions only. What is responsible for this quantity? The authors imply that it is measurement error, but no estimate of measurement precision is given in this manuscript. I find it rather unlikely that measurement error is responsible for this standard deviation. Rather, there are intermittent structures in the non-moist

environment that induce polarization. What are they? Is the atmosphere ever truly devoid of structures that induce polarization on GPS signals?

As it is stated in the last paragraph of section 4.1, the analysis is done using the m and σ for all the *no-rain* days. The standard deviation is defined as the square root of the average of the squared deviations from the mean, and it is also the square root of the variance. Even though the precision of the measurement could be quantified using the SNR information (as is done in *Cardellach et al. 2015*), other factors influence the actual precision of the measurement: there are residual time varying effects in the local multipath (for instance, changes in temperature that causes changes in the dielectric properties of the metals, which would slightly change the $\Delta\Phi$), small effects of the ionosphere, (even thought we assume here that these changes should be small), the stability of the emitted GNSS signal, and how perfectly RHCP it is (it is known that it exist a tolerance in the degree of polarization, but is not known). All of these effects, and maybe some others, slightly affect the signal, leading to an actual precision of the polarimetric phase shift measurements, after all our manipulations (removal of the mean, mutlipath, thresholds, ...) that has to be quantified empirically as it is done in the article. Thus, the standard deviation mentioned in the article (σ) refers to the dynamic range of the observations, what we assume to be the actual precision of our $\Delta\Phi_+$ measurement. No measurement error is given, and we have made changes in the text to state it more clear.
Regarding the atmosphere, to our knowledge, there should not be structures that induce noticeable polarization apart from the hydrometeors.

- Table 2: The authors conclude that atmospheric water meteors induce additional polarization to the GPS signal because the variance $\Delta\Phi_{day}^{PRN}(\varepsilon)$ corrected for rainy days is greater than the same for dry days. The authors should use the statistical **F-test** to establish a confidence level. Such a test determines whether or not two estimates of variance, each determined from a limited but different ensemble, are drawn from the same pool or not. It is ideally suited to this problem.

We want to thank the reviewer for suggesting this test. We have performed it and the results have been added in Table 2. The confidence level found is high, therefore our conclusions stand.

- Generally: What is the difference between “melting ice” and “graupel”?

Graupel forms when supercooled droplets of water freeze when they touch a falling snowflake, forming balls of rime. Here we have modelled “melting ice”, understood as a thin shell of liquid water surrounding an ice core. We simulate these particles to make it simple, and to have a representative particle for water, ice, and an intermediate stage.

- Equation 6 is incorrect. It should instead be $\Delta\Phi S\ \varepsilon = \Delta\Phi\ \varepsilon - (\Delta\Phi\ (\varepsilon min) + 2\sigma no\text{ - }rain\ (\varepsilon min))$

It has been corrected.

- Lines 21-23, p.18758: This analysis is odd. What is the statistical significance of this finding? If 82% of A! > 0 cases are rainy, are the other 18% of such cases dry? How many of the rainy cases had A! > 0? How many of the dry cases had A! > 0? Is this condition a strong test for the presence of rain?

The given numbers were slightly wrong. We found 28 rainy scenarios among the 30 $A_\Phi > 0$ measurements. The remaining 2 cases (7 %) are discussed at the end of section 5.3. Regarding the percentage of rainy cases that have $A_\Phi > 0$ measurements, we have not given the statistics because the processing applied in this experiment can actually bring A_Φ down. For example, when the polarimetric signature is constant during all the occultation, removing the mean we are killing this polarimetric signature. This is a particularity of this experiment. Also, small signatures could fall below the precision of the measurement.

- Figure 9 is illegible, as is Figure 11.

Figure 9 has been changed, and now is legible. Figure 10, 11 and 12 have been also changed, and we believe that now are easier to read and interpret.

- Regarding the ray-path simulator: Has it been validated against any data? Has there ever been a successful simulation of differential phase based on ground-truth atmospheric parameters, even in dry conditions?

The ray path simulator has been used before for standard radio occultation experiments, and its performance is good enough for the precision that we need here for the interpolations. Note that we only use the ray-tracer to estimate the path of the RHCP propagation (rays). Any polarimetric signature is added afterwards by modelling the hydrometeor effect at each point of the estimated RHCP ray trajectory. Also, interpolations rely on the weather information, which is available in discrete time steps. Thus, the simulation is affected by both ray tracing inaccuracies of the trajectory and time interpolation of the meteorological information.

Regarding the "successful simulation of differential phase", we are not sure what the reviewer is referring to:

In terms of the ray-tracer, it uses the actual atmospheric profiles retrieved by the radiosondes to generate the RHCP ray trajectories, thus the input information is ground-truth based. We also assume here that the interpolation made for the atmospheric parameters between radiosondes is enough for our purposes.

In terms of validating the measured differential phase, this is the first experiment using the GNSS signals taken at two polarizations, and therefore the only simulations of this kind are those in the article and those in *Cardellach et al. 2015.* Many similar studies but at higher frequencies have been performed, and some examples are given in Sec 1.

- Lines 13-14, p.18763: "Also, the model has been applied with the same..." I do not understand this sentence. What relation? What is an event? What are the conditions?

We have modified the sentence to better state the ideas

Manuscript prepared for Atmos. Chem. Phys.
with version 2015/04/24 7.83 Copernicus papers of the LaTeX class copernicus.cls.
Date: 17 November 2015

Atmospheric polarimetric effects on GNSS Radio Occultations: The ROHP-PAZ field campaign

R. Padullés[1], E. Cardellach[1], M. de la Torre Juárez[2], S. Tomás[1], J. F. Turk[2], S. Oliveras[1], C. O. Ao[2], and A. Rius[1]

[1]Institut de Ciències de l'Espai (ICE - CSIC / IEEC), Barcelona, Spain
[2]NASA Jet Propulsion Laboratory, California Institute of Technology, Pasadena, CA, USA

Correspondence to: Ramon Padullés (padulles@ice.cat)

Abstract. This study describes the first experimental observations showing that hydrometeors induce polarimetric signatures in Global Navigation Satellite System (GNSS) signals. This evidence is relevant to the PAZ Low Earth Orbiter, which will test the concept and applications of polarimetric GNSS Radio Occultation (RO) (i.e. ROs obtained with a two-polarization antenna). A ground field campaign was carried out in preparation for PAZ to verify the theoretical sensitivity studies about this concept (Cardellach et al., 2015). The main aim of the campaign is to identify and understand the factors that might affect the polarimetric GNSS observables. Studied for the first time, GNSS signals measured with two polarimetric antennas (H, horizontal and V, vertical) are shown to discriminate heavy rain events, by comparing the measured phase difference between the H and V phase delays ($\Delta\Phi$) in different weather scenarios. The measured phase difference indicates higher dispersion under rain conditions. When individual events are examined, significant increases of $\Delta\Phi$ occur when the radio signals cross rain cells. Moreover, the amplitude of such signal is much higher than the theoretical prediction for precipitation; thus other sources of polarimetric signatures have been explored and identified. Modelling of other hydrometeors like melting particles and ice crystals have been proposed to explain the obtained measurements, with good agreement in more than 90% of the cases.

1 Introduction

Global Navigation Satellite System (GNSS) Radio Occultations (RO) space-borne missions have been probing the Earth's atmosphere since 1995 (e.g. Rocken et al., 1997). They have been shown to be useful for climate monitoring (e.g. Steiner et al., 2011) and nowadays their thermodynamic profiles are being assimilated operationally into several numerical weather prediction (NWP) models (e.g. Healy et al., 2005; Cucurull and Derber, 2008).

A new measurement concept presented in Cardellach et al. (2015) aims at detecting and quantifying heavy precipitation events using polarimetric GNSS RO, by means of measuring the difference between the phase delays of the horizontal and the vertical components of the received propagated

signal. This technique will be tested aboard the PAZ Low Earth Orbiter (LEO) satellite with the RO and Heavy Precipitation experiment (ROHP-PAZ), and it will be the first attempt to detect rain using L band frequencies (1.575 GHz, i.e. $\lambda = 19.03$ cm). The launch is planned for ~~Q3 2015.~~ Q1 2016. The theoretical analysis performed in Cardellach et al. (2015) demonstrated not only that heavy rain events could be detected, but also that an approximated vertical structure of the rain cells could be retrieved.

Prior to the launch of the PAZ satellite, a field campaign has been conducted in order to study, for the first time, L1 occulting signals obtained at two polarizations, and start to identify and understand the factors that might affect the polarimetric signal. Placed on top of a mountain peak 1670 m above the mean sea level, the experiment was set up with an engineering model of the PAZ's polarimetric antenna pointing at the horizon and a commercial JAVAD receiver (provided by the German Research Center for Geosciences GFZ), enclosed in a shelter. A zenith-looking geodetic GNSS antenna has also been used for positioning. The RO antenna points south and to the horizon, and it tracks all the visible satellites in the East-West field of view from 0 to ~~20~~ 40 degrees of elevation and from 150 to 270 degrees of azimuth (see Fig.1). Although all the satellites are tracked simultaneously, only those crossing the main beam of the antenna are used in the posterior analysis. ~~These are the~~ For the time period analyzed, the GNSS satellites with highest number of samplings are the ones identified by the Pseudo-Random Noise (PRN) numbers G10, G14, G15, G22 and G31. Also, only the segments between 0 and 20 degrees of elevation are used for the analysis, since the antenna performance reaches its optimal values within this range. Given the geometry of the experiment's field of view, in most of the cases only one of either the descending or ascending trajectories over the horizon provided data within the antenna field of view.

The main objective was to collect a large amount of data free of rain, and to catch some heavy rain events in order to observe differences in the polarimetric observables between the two data sets. The area was chosen specifically for this purpose, given that the region is mainly dry and several intense local Mediterranean storms occur a few times per year (Ducrocq et al., 2014). The experiment ran for 8 months, from March 21st to October 10th in 2014. During this period, it collected data for about 170 days. There were about 25 days of rain, from which 5 could be considered heavy rain.

The geometry and measurements used for this experiment are closely related to those of the polarimetric weather radar observations. In the radar observations, the differential reflectivity (Z_{dr}) and the specific differential phase (K_{dp}) are the most important polarization signatures for rain characterization at low elevation angles (e.g. Bringi and Chandrasekar, 2001). Some differences apply in ~~our~~ this case: we are limited to one single observable, the differential phase between the H- and V-ports phase delay ($\Delta\Phi$), defined as:

$$\Delta\Phi = \int_L K_{dp} dl \tag{1}$$

where L is the path length under the influence of K_{dp}. The K_{dp} can be understood as a measure of the bi-refraction induced by hydrometeors that have an asymmetry between the horizontal and vertical axis and therefore a different effective propagation constant along them. Note also that K_{dp} is here defined in propagation (forward-scattering) rather than back-scattering. This is a one dimensional observation, since it is an integral along the ray path. Furthermore, the weather radars work with frequencies equal or higher than 3 GHz, thus the sensitivity to hydrometeors is expected to be higher than for the L-band signals.

From the polarimetric radar observations it is known that different kinds of rain, precipitation and particles could produce different K_{dp}. Studies for rain (e.g. Bringi and Chandrasekar, 2001; Trömel et al., 2013), ice (e.g. Vivekanandan et al., 1994; Ryzhkov and Zrnić, 1998), snow (e.g. Matrosov, 1992; Kennedy and Rutledge, 2011) and melting layer (e.g. Baldini and Gorgucci, 2006; Trömel et al., 2013) characterization using polarimetric observables have been widely conducted, as well as the continuous satellite observation of rain such as the Tropical Rainfall Measurement Mission (TRMM) and the Global Precipitation Mission (GPM) missions.

~~Therefore, our~~ Therefore, the aim here is not to characterize the different kinds of precipitation or hydrometeors, but to take advantage of this knowledge to understand ~~our~~ the observations.

This paper is organized in the following way: in section 2 the experiment geometry and the acquired data are described in detail, and a comparison with the satellite set-up is performed. Problems with the signal, local multipath characterisation, and expected improvements from satellite observations are addressed here. The collocated meteorological data used for validation are described in section 3. The statistical results of the experiment are shown in section 4, and a comparison with the forward model simulation results is performed in section 5. Finally, in section 6 the conclusions are discussed.

2 Polarimetric GNSS data

2.1 Observables

GNSS signal observables are the carrier phase and the pseudorange. In the standard RO, these are measured with a circular co-polar antenna (right-handed, as transmitted signals), and they are used to obtain the bending angle, which in turn is used to obtain the refractivity, pressure and temperature profiles (Kursinski et al., 1997). We refer to these as the standard RO thermodynamic profiles. The geometry found in the experiment is not a common RO configuration. Instead, ~~our~~ the receiver is inside the atmosphere, i. e. on the ground, and therefore the tangent point - LEO trajectory is missing (see Fig.2). The lack of symmetry and the non-existence of negative elevation observations does not allow us to retrieve the standard thermodynamic profiles (Healy et al., 2002), which are going to be retrieved from the satellite in the future experiment.

Also, the fact that the receiver is on the ground means that the radio-link is crossing all the atmosphere layers during all the observation time. In this configuration, the sounding of the atmosphere is different from a RO one. This has an important implication in ~~our~~ the observables.

The polarimetric GNSS observable $\Delta\Phi$ is the difference between the the carrier phase delay measured in the Horizontal (H) port and and the one measured in the Vertical (V) port. The observations in the H and V ports of the polarimetric antenna are independent, and therefore the receiver treats them separately. The GNSS receivers keep track of the total phase relative to their initial measurement, but the value associated with the first measurement is arbitrary (Blewitt, 1989). In this case, both signals (H and V) suffer from this ambiguity (phase ambiguity, ~~K~~ b) in their respective channel:

$$\begin{aligned}\Phi_i(t) &= \rho(t) + \rho_{atm}(t) + \rho^i_{hyd}(t) + \rho_{ion}(t) \\ &\quad + m^i(t) + d^i + C(t) + b^i \end{aligned} \tag{2}$$

where Φ is the measured carrier phase delay at the i port (H or V). ρ is the geometry range between the satellite and the receiver since the initial measurement (the same for H and V), ρ_{atm} ~~denote~~ denotes the delay due to the neutral atmosphere that is equal in the H and V channels, ρ_{hyd} is the phase delay due to the interaction with hydrometeors (the terms that we are interested in) and ρ_{ion} denote the ionospheric delay. m represents the local multipath in each component, the term d refers to the hardware effects of the receiver and the transmitter (such as noise, the effect of a possible difference in the cable's length, etc.) and C represents the clock drifts and errors. ~~K~~ b is the arbitrary initial constant that does not depend on time. Most of these terms are common in both components, thus the phase difference is:

$$\Delta\Phi(t) = \rho^H_{hyd}(t) - \rho^V_{hyd}(t) + m + Kb + d \tag{3}$$

where $m = m^H - m^V$, ~~$K = K^H - K^V$~~ $b = b^H - b^V$ and $d = d^H - d^V$.

We do not have sufficiently precise ~~L2~~ pseudorange measurements to solve the initial phase bias ~~using pseudoranges (~~as it is done in Blewitt (1989)~~). This term K ~~. The expected phase difference $\Delta\Phi$ is in the range of mm while the pseudorange accuracies are of the order of cm. This term b changes in every arc of data (continuous tracking) and therefore ~~our~~ the observation is not absolute, but relative to the first measurement.

To avoid further problems, we identify the ~~loss of tracks that occur during~~ breaks in the tracking of the same PRN, and we separate them in continuous arcs. Every time that the track is lost, the receiver starts again with a new arbitrary constant. For each day, we only consider the longest arc, and discard the rest.

To enable comparison among different observations, we force each arc to have a 0 mean:

$$\Delta\Phi'(t) = \Delta\Phi(t) - \langle\Delta\Phi(t)\rangle\,. \tag{4}$$

This step homogenizes all the observations ~~, and allows~~ allowing the comparison among them. It removes the contribution from ~~K b~~ and d terms, but it also erases any constant signature of the polarimetric measurement. Thus, any rain contribution in which depolarization is present since the beginning and remains until the end of the observation will be missed.

In a satellite to satellite geometry (PAZ scenario), even without knowing the arbitrary initial constants we expect to be able to calibrate the initial phase, since in the beginning of the occultation the radio-link between the GPS and the LEO is not crossing the atmosphere. A summary of the expected differences between the spaceborne mission and this ground experiment can be found in Table 1.

2.2 Local Multipath

~~Multipath~~ Local multipath is the result of the combination of the signal from the satellite and one or more signals from the same source that have followed different paths to reach the receiver, for example, being reflected on the ground or on a metallic structure. It affects the phase differently in the H and in the V components, giving a pattern that depends on the surrounding geometry, environmental conditions and position of the transmitter. ~~Our~~ The antenna is placed over a shelter, which has several metallic pieces. Also, there is a meteorological station a few meters from the experiment. Thus, ~~our~~ the data suffer from a severe local multipath. If the reflecting process affected equally both H and V, this effect would cancel in $\Delta\Phi$. However, metallic structures with longitudinal edges might differently affect the scattering in the two polarizations.

~~In similar environmental~~ The GPS satellites have an orbit period of one sidereal day. This implies that, in ideal conditions, the local multipath pattern ought to repeat after a sidereal day ~~(period of the GPS orbits), thus it can be characterized, and~~since the satellite is again in the same position with respect the observation site (it follows the same azimuth - elevation curve every sidereal day). To characterize and, to a large ~~extent, removed. We define our observations as~~ extend, remove the local multipath pattern from the signal, the time series of observations $\Delta\Phi_{day}^{PRN}(t)$ are converted into elevation series $\Delta\Phi_{day}^{PRN}(\epsilon)$. Time can be mapped into elevation using the GPS orbit information, that provides a precise GPS position for each time. This conversion allows the direct comparison among the observations from different days, making the signal only dependent on the satellite position. ~~This corresponds to one PRN arc for a specific day. In order to homogenise the samples, we convert time (t) to elevation (ϵ), since the same satellite has to be in the same position(i. e. elevation) after a sidereal day.~~

~~In ideal conditions, $\Delta\Phi_{day}^{PRN}(\epsilon)$ should be the same sidereal day after sidereal day. So, to characterize the multipath pattern, we perform~~ Once the direct comparison is possible, the local multipath pattern can be found performing the average and the standard deviation ~~as a function of elevation~~ of the $\Delta\Phi_{day}^{PRN}(\epsilon)$ for a given set of days. ~~We define~~ To account for all the environmental conditions in exception for rain, the local multipath pattern is obtained using all the days identified as *no-rain* days~~those days when no rain is present in the area, and *rain* days when the radar has detected~~

~~significant reflectivity (Z) nearby. The multipath pattern~~ . This identification is done taking into account information from two different sources: the ground weather station placed next to the observation site, and the radar reflectivity (Z_e) from the weather radar of the area. If the ground weather station indicates that no rain was accumulated during the observation time, and the weather radar indicates that no valid Z_e values were present between the antenna and the GPS, the day is labelled as *no-rain*. More details about the meteorological information used in the data analysis can be found in Sect. 3.

The average (m) and ~~its~~ the standard deviation (σ) ~~for~~ of the *no-rain* days ~~for a certain PRN~~ ($m^{PRN}_{no-rain}, \sigma^{PRN}_{no-rain}$) represent the local multipath pattern for *no-rain* days and can be seen in Fig. 3 top. Note that the multipath pattern features vary between GPS transmitters, because of different geometry, thus interaction with the nearby structures. Usually, $\sigma^{PRN}_{no-rain}$ is large at low elevations. This is due to a lower quality of the signal, that has travelled ~~through longer~~ a longer time through the atmosphere layers than those rays at higher elevations.

To obtain the final measurement, i.e. the one that will be analysed, this local multipath pattern is removed from the measured signal $\Delta\Phi'(\epsilon)$:

$$\Delta\Phi^{PRN}_{day}(\epsilon)\Big|_{corrected} = \Delta\Phi^{PRN}_{day}(\epsilon)\Big|_{observed} - m^{PRN}_{no-rain}(\epsilon)\,. \tag{5}$$

The antenna pattern is also affecting the measurements differently in each component ~~.~~ and induces a phase difference due to its different response to each polarization. Since the antenna is the PAZ's engineering model, the characteristics should be the same as the one mounted in the satellite and its pattern is characterized in Cardellach et al. (2015). Its effect, though, is implicitly taken into account in the $m^{PRN}_{no-rain}$ term (it is constant in time and only depends on the satellite position), and therefore it is implicitly corrected applying Eq. 5.

Hereafter, the corrected measurement will be referred as $\Delta\Phi^{PRN}_{day}(\epsilon)$. An example of corrected $\Delta\Phi^{PRN}_{day}$ is given in Fig. 3 bottom.

2.3 Ionosphere

It is well known that the ionosphere affects the GPS signal carrier phase delays and pseudorranges. In terms of polarization, there are two effects that have an effect on the signals~~:~~, the Faraday rotation and the Cotton-Mouton effect. The Faraday rotation is due to the longitudinal component of the Earth magnetic field (longitudinal here meaning along the signal propagation direction), while the Cotton-Mouton effect is due to its transverse component (perpendicular to the propagation direction).

Faraday rotation changes the polarization axis of the propagating signals, proportionally to the total electron content (TEC) crossed and the longitudinal component of the Earth magnetic field. ~~Yet, the~~ If the signal is transmitted at pure right hand circular polarization (RHCP) then the rotation

angle effect is the same in both components, H and V, and therefore it should not be noticeable when differentiating both signals.

On the other hand, the Cotton-Mouton effect could induce different phase delays in each component~~(e.g. Zhang et al., 2010). However, the effect is expected to be small enough to be negligible~~. According to Yeh et al. (1999), under the Earth's ionospheric conditions and frequency bands higher than 25 MHz, the Cotton-Mouton effect becomes significant only when the magnetic field is almost perpendicular to the propagation (see Figures 4a and 5a, for 25MHz and 1MHz in the aforementioned reference). Otherwise, only the longitudinal (Faraday rotation) is relevant. For example, despite the magnetic field being ~ 80 deg. from the propagation, the Cotton-Mouton effect is still negligible.

~~A summary of the expected differences between the spaceborne mission and this ground experiment can be found in table 1.~~ Given the geometry of the GPS orbits, the experimental site location and antenna boresight orientation, these conditions ($\mathbf{B}$ at ionospheric altitudes perpendicular to GPS signal propagation) did not happen. Note that even for a LEO in polar orbit (such as PAZ polarimetric-RO experiment will be) the probability to find $\mathbf{B}$ perpendicular to the propagation direction is small.

2.4 Measurement precision

Even though the carrier phase measurement precision could be determined as in Cardellach et al. (2015), this would not be an actual value for the real precision of the polarimetric phase shift measurement in this experiment. Many factors, such as multipath, add dispersion to the observations and affect the actual precision of the measurement. These effects cannot be theoretically characterized and removed, but they have to be empirically determined.

Besides multipath, other effects are, for instance, a non-perfectly circular polarization of the emitted signals, which could lead to small polarimetric ionospheric effects (the waves emitted by the GPS satellites are in principle perfectly RHCP, but they admit a small tolerance). Also temperature variations in the surrounding could change the dielectric constant of the media, and therefore slightly modify the multipath pattern day after day. Among others, these effects add dispersion to the polarimetric phase shift measurement and cannot be disentangled among them. Therefore, they end up included in the $\sigma^{PRN}_{no-rain}$ term in Eq. 5.

3 Meteorological weather data

The objective of ~~our~~ the analysis is to understand the new polarimetric observations, which requires collocated meteorological information. ~~We have been provided by the data from the weather radars~~ The weather radar of the area, ~~data from the METEOSAT satellites and data from radiosondes~~in-situ radiosonde data and METEOSAT satellites measurements near the GNSS observational site are used in this study.

The Servei Meteorològic de Catalunya (METEOCAT) has a weather radar network covering the Catalan coastal area (Bech et al., 2004). We have access to the data from one of the radars, which has full coverage of the area under study. These radars are all Doppler systems, with one single polarization, operating at C-band (5.6 GHz). The provided data consists of the radar reflectivity (~~Z~~Z_e) in dBZ, as a function of latitude, longitude and height. Its resolution is $1 \times 1 \times 1\ km$ in a grid of $300 \times 300\ km$, per 10 km of height, and every 6 minutes. Since it is not a polarimetric radar, we can not extract information such as K_{dp} or Z_{dr}, which would provide clues about the orientation of the particles. The minimum Z_e value that is considered valid is 0 dBZ, below that the signal is considered noise and it is removed.

METEOCAT ~~has also~~ also has a network of ground stations that provides the accumulated precipitation, temperature and relative humidity in 30 minutes batches. ~~One of them is a few meters from our antenna.~~ In a radius of 30 ~~kms~~km around the observation site, there are ~~4 more ground stations~~5 ground weather stations, with one locating a few meters from the GNSS antennas. Through them we can have an approximation of the surface rain rate during the rain events.

Besides the radar and ground stations data, Cloud Type (CTY), Cloud top Phase (CP) and Cloud Top Height (CTH) data products from the ~~Support to~~ Nowcasting and Very Short Range Forecasting (NWC-SAF) have been used. The data have been provided by the Agencia Estatal de Meteorología (AEMET) and the European Organisation for the Exploitation of Meteorological Satellites (EUMETSAT). These data ~~results from the~~ products are a combination of satellite ~~imagery~~ observations and Numerical Weather Prediction (NWP) ~~inputs. It is~~ model simulations. The satellite observations are obtained by the MSG stationary meteorological satellites. They measure brightness temperatures and radiances with a radiometer at 12 different wavelengths (4 ranging from 0.4 to 1.6 μm and 8 ranging from 3.9 to 13.4 μm). The horizontal resolution is $\sim$ 3 km and the products are available for the study area every 15 minutes (Aminou, 2002).

~~Using the CTYand CP products we can know the cloud top phase and using the CTHproduct we can know the height of the top of the cloud. Combining this information we can properly collocate our observations.~~ The collocated cloud observations from NWC-SAF (CTY, CP and CTH) are then interpolated with the GNSS ray trajectories. Unfortunately, these sets of data do not provide information about the orientation of the ice particles. Only those with its major axis oriented horizontally would induce a positive polarimetric signature. These data is mainly used to identify the top of the clouds, and to identify ice above the maximum radar products height.

To complement all the information we use the measurements provided by METEOCAT's radiosondes. These radiosondes are launched two times per day (00 and 12 UTC) at a distance of approximately 50 km to the South-East of ~~our~~ the antenna, and provide temperature, pressure and humidity as a function of height. ~~Even though the temporal resolution is not very high, approximated~~ With the limited two-time daily soundings, the temperature and refractivity ~~vertical profiles are~~

~~obtained interpolating both radiosondes, weighting their information with the time difference~~profiles can be interpolated into the GNSS observation time.

Once all the information is recompiled, we can perform ~~an exact collocation of the~~ exact collocations of the GNSS polarimetric observations with the weather data. To do so, we first simulate the rays from the GPS to the antenna using a ray-tracer called OAT, which solves the trajectory of each ray across the atmosphere characterized by the retrieved refractivity profiles (Aparicio and Rius, 2004). An illustration of the performed collocation can be seen in Fig. 4. Then, we interpolate all the weather information for each of the points of the ray trajectory. For this analysis, each ray consists of 500 points, separated $\sim 0.52\ km$ among them. We simulate 501 rays, between 0 and 20 degrees of elevation.

4 Statistical results: Do rain induce polarimetric features?

4.1 ~~Standard~~ Polarimetric signatures in $\Delta\Phi$ standard deviations

Once the data have been pre-processed as described in Sect. 2, the analysis should determine whether the corrected $\Delta\Phi^{PRN}_{day}(\epsilon)$ is affected by rain or not.

~~First of all, an analysis of the standard deviation is performed.~~ To do so, corrected $\Delta\Phi^{PRN}_{day}$ are grouped ~~in three sub-sets~~according to three different meteorological conditions. For each ~~sub-set~~ group, the standard deviation as a function of elevation ~~$\sigma^{PRN}_{subset}(\epsilon)$ is computed~~$\sigma^{PRN}_{met}(\epsilon)$ is computed. The three meteorological conditions and the corresponding σ are:

- Dry days: days when the observation was made in a low relative humidity conditions (i.e. the relative humidity has not reached 100%) according to the nearby weather ground station, and without rain $(\sigma^{PRN}_{dry}(\epsilon))$. No rain is stated when the nearby weather ground stations do not accumulate any rain during the observation time and the interpolation of the weather radar data along the GNSS rays does not cross any area where valid Z_e values (Z_e>0) are detected.
- Wet days: days either with hight relative humidity (i.e. the relative humidity has reached 100%) according to the nearby weather ground station during or before the observation; or rain before or after the observation; or both $(\sigma^{PRN}_{wet}(\epsilon))$.
- Rain days: Days ~~with rain in the surroundings during the observation time~~ when the GNSS rays have crossed an area where valid Z_e values are detected by the weather radar $(\sigma^{PRN}_{rain}(\epsilon))$.

This classification has been done in order to compare different ~~environmental situations~~meteorological conditions. For example, high relative humidity conditions could have caused condensation, leading to a wet soil and different local multipath and antenna behaviour. The ~~results of~~ mean σ ~~averaged for all elevation angles, for several PRNs and for the three day sub-sets~~ across all elevation observations for each GNSS satellite during the three different meteorological conditions are summarized in Table 2.

It can be seen that *dry* days present always a lower σ than the rest, and that *rain* days exhibit the largest σ. The standard deviation for *wet* days is also larger than for *dry* days, but the difference is less significant than for the *rain* days. There should not be any significant differences between *wet* and *rain* days, in terms of the surroundings condition. For example, just after rain, the soil should be as wet as during the rain. Therefore, the ~~largest~~ larger σ ~~that~~ in *rain* days comparing with the *wet* days indicates other factors should have contributed to the enhanced polarimetric signature other that the enhanced local multipath due to the wet soil in the *rain* days~~show could mean that under rain conditions, the signal is affected by something else than for different multipath.~~ .

To check if this difference is enough to be treated as different populations (i.e the cause of the different standard deviations is that we are under different scenarios and not due to a different sampling) a simple statistical test called F-test is performed (Walpole et al., 2012). We define the *f* statistic as the ratio of the variances (σ^2) of the populations that we are comparing, the P_F as the cumulative probability of *f*, and we compare the *rain* days with the *no-rain* days, where the *no-rain* are all the *wet* and *dry* days. The results of P_F are shown in Table 2. It can be understood as the significance level that we are rejecting the null hypothesis, that in this case is that the variances that we are comparing come from the same pool. It can be seen that 4 out of the 5 analysed PRNs have a P_F large enough to state that there exist a difference in the standard deviation that could be related to rain.

Hereafter and for the rest of the analysis, the correction of the $\Delta\Phi^{PRN}_{day}(\epsilon)$ is done as described in Eq. 5 using $m^{PRN}_{no-rain}$, which is computed as in Sec. 2.2 accounting for all the *dry* and *wet* days defined ~~here to calculate $m^{PRN}_{no-rain}$~~ in this section together.

4.2 Phase difference as a function of elevation

Examining each event individually, more features can be observed. To do such analysis, we compare each observation $\Delta\Phi^{PRN}_{day}(\epsilon)$ with the $\sigma^{PRN}_{no-rain}(\epsilon)$. We define a $2\sigma^{PRN}_{no-rain}$ threshold to detect polarimetric signatures in the signal: statistically speaking, $\sim 95\%$ of the data should be within $\pm 2\sigma^{PRN}_{no-rain}$. Thus the remaining 5% of the data points and those affected by some polarimetric feature should lay beyond $\pm 2\sigma^{PRN}_{no-rain}$.

Lacking an absolute reference for the phase difference and to identify points overpassing the $\pm 2\sigma^{PRN}_{no-rain}(\epsilon)$ threshold, we find the elevation point where the difference between $\Delta\Phi^{PRN}_{day}(\epsilon)$ and $-2\sigma_{no-rain}(\epsilon)$ is minimum, and we identify it as ϵ_{min}. Then, we subtract this difference from the observation, and what ~~we obtain is~~ is obtained is the observation aligned in a way that for each event its minimum lays on the line of $-2\sigma_{no-rain}$ threshold:

$$\Delta\Phi_S(\epsilon) = \Delta\Phi(\epsilon) - \left(\Delta\Phi(\epsilon_{min}) \mp 2\sigma_{no-rain}(\epsilon_{min})\right) \tag{6}$$

Defining $2\sigma^{PRN}_{no-rain}(\epsilon)$ as the no-rain noise level, $\Delta\Phi_S$ can be understood as a bias-corrected settled phase difference. After this correction, we can easily detect the points outside the 2σ thresh-

old. The region of $\Delta\Phi_S(\epsilon)$ above the $+2\sigma_{no-rain}$ threshold is defined as follows:

$$\Delta\Phi_+(\epsilon) = \begin{cases} \Delta\Phi_S(\epsilon) - 2\sigma(\epsilon) & \text{if} \quad \Delta\Phi_S(\epsilon) > 2\sigma(\epsilon) \\ 0 & \text{if} \quad \Delta\Phi_S(\epsilon) \leq 2\sigma(\epsilon) \end{cases} \tag{7}$$

~~And the area of $\Delta\Phi_+(\epsilon)$~~ $\Delta\Phi_+(\epsilon)$ would be the phase difference above the statistical no-rain noise level and its area is defined as A_Φ:

$$A_\Phi = \int \Delta\Phi_+(\epsilon) d\epsilon \tag{8}$$

An example of $\Delta\Phi_S(\epsilon)$ and A_Φ is shown in the bottom plot in Fig.5. In this procedure, we only consider the option of positive phase differences, as it is expected for rain effects (Cardellach et al., 2015).

We have found ~~28~~ 30 observations with $A_\Phi > 0$, of which ~~82%~~ 28 correspond to rainy scenarios. This ~~represents the first experimental confirmation of the theory that precipitation conditions induce polarimetric features in~~ is the first direct observational evidence of the polarimetric signatures induced by precipitation conditions in the GNSS signals.

5 Are the observed polarimetric features consistent with the models?

In order to explain the observations, forward scattering calculations have been performed. The aim is to simulate the effect of several kinds of hydrometeors, such as rain drops, pristine ice particles and melting ice particles, to cross-compare with weather radar reflectivities, satellite observations and the phase differences measured.

First of all, the K_{dp} and the radar reflectivity factor (Z_e) have been calculated for each hydrometeor type. These calculations have been done using the DDScat code (Draine and Flatau, 1994, 2013).

DDScat provides the phase lag efficiency factor (Q_{pha}) for each polarimetric component H and V. It is related to the forward scattering amplitude f_{sca} through $Q_{pha} = \frac{2\pi}{k} \frac{\Re\{f_{sca}\}}{\pi a_{eff}^2}$. Thus, it can be used to calculate the K_{dp}:

$$K_{dp} = \frac{\lambda}{2\pi} \int \left(Q_{pha}^H - Q_{pha}^V\right) \pi\, a_{eff}^2\, N(D)\, dD \tag{9}$$

where a_{eff} is the equivolumetric radius of the particle, $N(D)$ is the particle size distribution, D is the equivolumetric diameter and K_{dp} is in mm/km.

DDScat also provides the differential backscattering cross section normalized by πa_{eff}^2:

$$Q_{bk} = \frac{1}{\pi a_{eff}^2} \frac{\partial \sigma_{sca}}{\partial \Omega}\Big|_{\Theta=180} \tag{10}$$

The backscattering cross section can then be obtained:

$$\sigma_{bk} = 4\pi Q_{bk} \pi a_{eff}^2 \tag{11}$$

Using the σ_{bk} ~~we can calculate ,~~ the radar reflectivity factor Z_e can be calculated as follows:

$$Z_e = \frac{\lambda^4}{\pi^5 |K_w|^2} \int_0^{D_{max}} \sigma_{bk}(D) N(D) dD \tag{12}$$

where λ is the wavelength, ~~K_w is $(m_w^2 - 1)/(m_w^2 + 2)$~~ $K_w = (m_w^2 - 1)/(m_w^2 + 2)$ and m_w is the complex refractive index of water (Smith, 1984).

K_{dp} is calculated for L-band frequency (GNSS observations), and Z_e for C-band frequency (weather radar observations). ~~The reason is that we want~~ This will allow to relate the reflectivity ~~obtained by the meteorological weather radar , that operate at~~ from the weather radar in C-band ~~, with our observations~~ with the GNSS observations in L-band.

The $N(D)$ that has been used is a gamma function of the form:

$$N(D) = N_0 D^{\mu} e^{-\Lambda D} \tag{13}$$

where N_0 is the scale parameter, Λ is the slope parameter and μ is the shape parameter (Ulbrich, 1983). These are the 3 parameters of the gamma $N(D)$. The particle size distribution ~~determines other quantities through its moments,~~ can be used to determine other quantities such as the K_{dp} (e.g. Eq.9), Z_e (e.g. Eq.12), liquid or ice water content (LWC, IWC), effective particle diameter (D_{eff}), mean weighted diameter (D_m) and rain rate (R). Further details of the relation between these magnitudes and the ~~moments of~~ $N(D)$ can be found in the literature, for example in Williams et al. (2014).

Since there is not a unique parameterization of the $N(D)$ that apply to all scenarios, we generate a set of mathematically valid $(N_0, \Lambda, \mu)^i$ triplets, each one producing a different $N(D)^i$. Then, each triplet has an associated physical magnitude:

$$(N_0, \Lambda, \mu)^i \rightarrow N(D)^i \rightarrow (K_{dp}^i, Z_e^i, LWC^i, D_{eff}^i, D_m^i, R^i, ...)$$

Depending on the hydrometeor being modelled, not all $N(D)$ parameters will be physically consistent, that is, fall in ranges that have been observed amongst various ground validation data (Williams et al., 2014). In the next section we describe the selection criteria for the valid ranges to choose among the possible $N(D)^i$.

5.1 Modelled A_Φ: rain ~~effect~~effects

At the beginning of the campaign, only rain was expected to affect the polarimetric signal. To simulate the polarimetric rain effect, the Q_{pha} and σ_{bk} have been calculated with DDScat using the predetermined oblate spheroid shapes, with D ranging from 0.1 to 6 mm, and Axis Ratio (AR) following the Beard and Chuang (BC) relation (Beard and Chuang, 1987), as it was done in Cardellach et al. (2015). Shape is sketched in Fig 6 (left). Some constraints have been applied to the (N_0, Λ, μ) triplets in order to use only those producing physically valid quantities: we have limited R to be

as high as 70 mm/h ~~because the observations from the~~ as suggested by the meteorological ground stations~~suggest so, and we have limited the~~ , and an upper limit of LWC ~~to be smaller than~~ is set to be 3 g/m^3 ~~, as an upper limit that is in agreement with the observation~~ according to the observational evidence of severe storms described in Black and Hallett (2012). All the parameter triplets producing quantities out of these ranges are discarded.

From the chosen $N(D)$ we derive Z_e and K_{dp}. All the valid Z_e^i and K_{dp}^i for rain conditions are shown in black in Fig. 7. To relate the observations from the weather radar and the measurements from the polarimetric antenna, we need to use a $Z_e - K_{dp}$ relation. It can be seen in Fig. 7 how a wide range of possible K_{dp} can be related to a given Z_e. For simplicity, we will use the $Z_e - K_{dp}$ indicated with a thick line in Fig. 7.

We have simulated the expected A_Φ caused by rain for every GNSS measurements, using the radar Z_e values interpolated to GNSS ray trajectories, and this $Z_e - K_{dp}$ relation. The results can be seen in black dots in Fig. 8. Despite the polarimetric signatures happening on rainy days, Fig. 8 shows that rain drops alone do not induce the large polarimetric signals observed ~~.~~ (black dots in Fig. 8). Therefore, the effects of other hydrometeors must be taken into account.

5.2 Could ice and melting particles explain the large polarimetric signatures?

We aim here to simulate the expected A_Φ induced by icy and melting particles. To simulate the ice particles, dendritic shapes have been used. Their characteristics are described in ~~?~~Liu (2008). For melting ice particles, two concentric ellipsoids have been used: the inner one made of pristine ice and the outer one of water. Both have the same axis ratio, ranging from 0.1 to 0.8, and with D ranging from 0.01 to 6 mm. The water shell is considered to range between a 5 and a 10 % of the volume of the inner core. Their shapes are sketched in Fig 6 (center and right).

A given ice-induced Z_e can be explained by a diversity of ice particle characterizations, such as different combinations of canting angle, IWC, percentage of horizontally oriented particles with respect to randomly oriented ones, or predominant sizes of the particles, among others. This diversity of ice conditions relate to a diversity of K_{dp}. This means that a given Z_e links to many possible K_{dp} values. Since we want to keep this modelling simplistic to understand the contributions and an order of magnitude of the polarimetric effect, and because we do not have ancillary information to properly characterize the ice properties, we have simulated this effect using only horizontally oriented dendrites, with a maximum IWC of 1 g/m^3. Horizontal orientation is supported by many studies, for example Matrosov and Mace (2012) or Noel and Chepfer (2010). The ~~chosen~~ IWC maximum is chosen accordingly to the maximum values observed in Delanoë and Hogan (2010). The chosen Z_e^i and K_{dp}^i for ice particles are shown in Fig. 7 in blue, and the $Z_e - K_{dp}$ relation used for ice particles is highlighted with a thick blue line.

Melting ice particles have even a wider range of variability. As can be seen in Fig. 7 (in gray), the possible Z_e^i and K_{dp}^i are widely spread. We have used the $Z_e - K_{dp}$ relation indicated with a gray

thick line when accounting for melting ice particles. As for rain and pristine ice, this relation is rather arbitrary, as we do not have the required ancillary ground-truth information to properly characterize these particles, and ~~our~~ the goal is to explain, to an order of magnitude, ~~what we have measured~~the measurements.

We have separated the contribution of rain, ice, and melting ice particles according to the temperature. The temperatures are given by the METEOCAT's radiosondes, mentioned in Sect. 3. Noting that the radiosonde observation may differ in exact location and time, they are the closest to a true value of the temperature profiles. These radiosonde observations are on the GPS antenna field of view. For the cells above land (like the ones analysed here), METEOCAT profiles are less than 50 km away and temperatures above the boundary layer should be representative. The radar reflectivity measured at heights with temperatures above $1°C$ is considered to come from rain. Particles in the range between $1°C$ and $-5°C$ are assumed to be melting ice particles. Below $-5°C$ they are assumed to be ice. Ice particles are assumed to be bigger in the range between -5 and -20 $°C$, because this region is considered to be the maximum dendritic growth zone (Kennedy and Rutledge, 2011).

Above the radar measurements, ice contributions are assumed when the simulated ray intersects with ice regions, according to the combination of the Cloud top Phase and Cloud Top Height products from the NWC-SAF. In this case, the particles are assumed to be smaller. We assume a thickness of the ice particle layer of about 2 km, in agreement with Noel and Chepfer (2010).

In addition, the contribution to A_Φ due to ice and melting particles is only simulated when the observed $\Delta\Phi_+(\epsilon)$ is positive. The reason is that if there were no measurement of $\Delta\Phi_+(\epsilon)$, there would not be oriented crystals in the ray path, nor a contribution to K_{dp}. The Cloud-Aerosol Lidar and Infrared Pathfinder Satellite Observations (CALIPSO) images show how only some regions of the clouds contain oriented ice crystals. This is consistent with discontinuous positive observations of $\Delta\Phi$, as is observed here. Unfortunately, no collocations were found between CALIPSO and the experiment.

The results for the simulated A_Φ taking into account the different hydrometeors are shown in orange dots in Fig. 8.

For every black dot (only rain simulated) an orange dot is included. Since they try to reproduce the same observed A_Φ, there will be a black and an orange dot for every observed A_Φ. A block diagram is shown in Fig. 9 to help the reader follow the steps that lead to the Fig. 8 results. All the data, information and relations used from the data acquisition to the final results are summarized in it.

~~One~~ Comparing the corresponding black and orange dots for a given observed A_Φ, one can notice how the simulated A_Φ increases significantly using all three hydrometeor types with respect to using only rain. ~~In~~ Also, in most of the cases ~~,~~ the simulated A_Φ is larger than the measured one ~~. As we have said, the model~~ (see the slope of the best fitted lines, dot-dashed in Fig. 8). This means

that we tend to overestimate A_Φ in the simulations. Indeed, the particle characteristics that we have used ~~is very simple, and the modelling of ice crystals and melting ice particles has assumed very favourable conditions, like the~~ in the simulations may increase the K_{dp}: the orientation of the particles ~~without canting angle, or the lack of other kind of particles (i.e. aggregate shaped), which would reduce significantly their contribution to the K_{dp}. Also~~is assumed to be horizontal (maximizing the polarimetric effect), and the type of particles is taken to be very asymmetric (when reality is more diverse).

Moreover, the model has been applied ~~with~~ using the same $Z_e - K_{dp}$ relation for each hydrometeor type, ~~although every event has its own conditions.~~

~~In addition, the contribution to A_Φ due to ice and melting particles is only simulated when the observed $\Delta\Phi_+(\epsilon)$ is positive. The reason is that if there were no measurement of $\Delta\Phi_+(\epsilon)$, there would not be oriented crystals in the ray path, nor a contribution to K_{dp}. The Cloud-Aerosol Lidar and Infrared Pathfinder Satellite Observations (CALIPSO) images show how only some regions of the clouds contain oriented ice crystals. This is consistent with discontinuous positive observations of $\Delta\Phi$, as is observed here. Unfortunately, no collocations were found between CALIPSO and our experiment.~~

~~The goal of this exercise has been to check if the measured $\Delta\Phi$ (and therefore A_Φ) can be explained by adding the contribution of these hydrometeors to the rain contribution, that by itself underestimated the polarimetric signatures. The results shown in Fig. 8 confirm that adding other hydrometeors in the model increases A_Φ. The $Z_e - K_{dp}$ relations used favoured high K_{dp} and hence high A_Φ for a given Z_e, which explain why orange dots tend to overestimate A_Φ~~in every analysed rainy event. Fine tuning of the parameters for each individual observation would be needed in order to fairly reproduce the observations, but this ~~is not our aim here, nor would it~~ would not be possible to validate ~~such tuning~~ due to the lack of ancillary independent information~~.~~, and it is thus beyond the scope of this work. Yet, it can be seen how the inclusion of icy and melting particles besides rain can explain the order of magnitude of the observations.

5.3 Illustration cases

In order to further check the internal consistency of the measurements, ~~we compare~~ a comparison among several observations for different PRNs ~~in the same day~~is performed, during the evolution of heavy rain episodes. In this section we analyse three ~~such episodes.~~ of such episodes: events on 2014/06/14, 2014/08/22 and 2014/05/26. To do so, we show the weather radar data, the observed phase difference above the noise level ($\Delta\Phi_+$) and the simulated $\Delta\Phi_+$. An example can be seen in Fig. 10. It corresponds to PRN 22 on 2104/06/14.

The ~~collocation of the ray trajectories with the radar reflectivity are shown for each day and observation,~~ figure shows each GNSS ray identified by its elevation angle. Every point along the ray is associated with its height (left Y axis) and it is coloured according to the corresponding radar

reflectivity Z_e (from the interpolation between the GNSS rays and the weather radar). Besides that, every elevation angle is associated to a $\Delta\Phi_+$ measurement (it is an along-ray integral measurement) and it is plotted as a thick black line that is ruled by the right Y axis. The simulated $\Delta\Phi_+$ is plotted with dashed lines along with the measured $\Delta\Phi_+$, and ~~superimposed there is the $\Delta\Phi_+$. For clarity purposes, in Figure 10 we only show one illustrative case and the caption details how to understand the plots. Then, the~~ is also ruled by the right Y axis. Therefore, in these figures it can be shown the measured phase difference plotted overlaying the radar reflectivity that is inducing it, and a comparison with the results of the simulation. A temporal series of such plots along heavy rain episodes are shown in Figures 11 and 12.

Figure 11 corresponds to events on 2014/06/14, 2014/08/22 and 2014/05/26, ~~respectively.~~ (same day represented in the same column) respectively:

- In the case of 2014/06/14, according to the nearby meteorological ground stations, there were maximum accumulations of rain of 14 mm in 30 minutes. This corresponds to peaks of ~~R~~ rain rate higher than 28 mm/h. ~~It can be seen how~~ Large positive $\Delta\Phi$ is present ~~mainly when larger amount of Z~~ when large radar reflectivity (Z_e) is accumulated at high altitudes. This is in agreement with the fact that rain alone produces lower polarimetric signatures than the ones detected with the present configuration.

- On 2014/08/22, the nearby meteorological ground stations suggest ~~R~~ peaks of rain rate higher than 55 mm/h according to the accumulated precipitation over 30 minutes. As in the previous case, positive $\Delta\Phi$ measurements are observed in the regions where significant ~~Z~~ Z_e reaches high altitudes, and where the temperature is around or below 0 $^\circ C$ (ice and melting particles).

- The last case, on 2014/05/26, there were not such high ~~R~~ rain rate peaks, but significant ~~Z~~ Z_e is also present at high altitudes, in agreement with the positive $\Delta\Phi$ observations.

Among all the studied cases (30), more than ~~90%~~ 93% (28) can be explained with the combined hydrometeor modelling~~.~~, i.e. the modelling can reproduce the order of magnitude of the observations. An example of ~~these cases which~~ one of the two cases in which the simulations failed to explain the observations can be seen in Fig. 12, on 2014/07/09. In this case, positive $\Delta\Phi$ measurements can not be associated with any significant radar reflectivity, nor to ice in the tops of the clouds crossed by the ray. ~~More specifically, the positive $\Delta\Phi$ measured while tracking PRN $G15$ remain unclear, so far~~Possible explanations could be some discrepancies due to missing observational data in the radar, or errors in the temperature (that relies in the radiosonde interpolation) that might lead to a bad hydrometeor identification.

6 Conclusions

For the first time, GNSS occulting signals have been acquired using a two polarization antenna ~~with the aim of detecting rain. This~~ and the evidence of the polarimetric signature induced by hydrometeors in the GNSS signals has been presented. The technique, presented in Cardellach et al. (2015), will be tested from space aboard the PAZ Low Earth Orbiter. If successful, it will be possible to provide rain flags, and potentially information about rain structures, collocated with the standard RO thermodynamic profiles.

The experiment presented here was intended to characterize the phenomena that are actually affecting the polarimetric signatures. It has consisted of comparing the measurements of the polarimetric observable $\Delta\Phi$ under different weather conditions, trying to identify rain signatures. Data from ~~6~~ 5 GNSS transmitters on ~ 170 different days have been analysed.

Many challenges have arisen in the data analysis process. Three main issues affect the data: the location of the antenna/receiver (low inside the atmosphere, not proper RO geometry), the phase ambiguity problem (linked to internal processing of the commercial receiver~~, out of our control~~), and severe and varying local multipath (mostly due to the nearby environment, metallic towers and structures). ~~None of these effects are~~ These effects are not expected (or ~~not as severely~~milder) in the spaceborne mission: Regarding the location of the antenna/receiver, the future experiment will be in the space, and therefore outside the atmosphere. Being outside the atmosphere will allow a better calibration of the signals thanks to the scanning geometry: a vertical descent from the outer layers approaching the Earth surface. Thus, at the beginning of the observation there are no depolarizing effects, and it will be possible to define the initial state (calibration of the polarimetric phase measurement). Phase ambiguity will be solved, and absolute measurements will be possible, unlike in this experiment. Also, in the satellite we expect the local multipath to be smaller, and most importantly, it will not change with the environmental conditions.

After analysing the data, two main conclusions can be extracted.

In a general view, rain scenarios affect the polarimetric observables. The standard deviation of the mean $\Delta\Phi$ for *dry*, *wet* and *rain* days have been examined. For environmental reasons (wet soil, increase of the reflectivity, etc.), the σ for *wet* and *rain* days is higher than for *dry* days. However, the increase of the σ_{rain} with respect σ_{dry} is between 20 and the 40% larger than the increase of σ_{wet} with respect σ_{dry}.

This could empirically answer one of the questions that we were seeking for an answer: Are radiolinks crossing rain cells affected by any depolarization affect? And if so, is it detectable? According to the σ behaviour under the different weather and environmental conditions, we can answer that under rain scenarios, the measured $\Delta\Phi$ suffer from higher variability, and the difference from other scenarios is noticeable.

A more detailed analysis of the $\Delta\Phi(\epsilon)$ has been performed for each individual observation. $\Delta\Phi$ above the defined 2σ threshold, and the computed A_Φ have been compared with simulated results.

Simulated K_{dp} using the collocated radar reflectivity has shown that rain drops induce an effect much lower than ~~our~~ the measurements. This indicates that other phenomena are inducing polarimetric signatures too. This is an important point in views to the future analysis of the spaceborne ROHP-PAZ data.

Ice crystals and melting ice particles have been added to the modelling, using temperature information and satellite imagery to distinguish between hydrometeors. Simulations of these particles have been kept very simplistic, due to the number of possible parameters involved in the modelling and the lack of information to validate them. ~~Our~~ The goal at this stage is to identify the sources of polarimetric signatures. The simulations have shown that, in most of the cases, the measured $\Delta\Phi$ could be explained by the K_{dp} induced by all possible hydrometeors.

Simulated $\Delta\Phi$ and A_Φ with all the hydrometeors are usually above the measured values. Fine tuning of the parameters involved in the modelling would be needed in order to match the observations, but ~~we feel that this would be too speculative and~~ nevertheless impossible to validate in this particular experiment.

Microphysical analysis of the precipitation and inversion procedures development are left for later studies with RO, data more suitable than mountain-top occultations. Yet, the results obtained here represent the first empirical evidence that hydrometeors induce measurable polarimetric signatures in occulting GNSS signals after the theoretical analysis in Cardellach et al. (2015). These results are helping us to understand the types of processes affecting the data from the future polarimetric RO experiment aboard PAZ. They additionally show the potential capability of polarimetric RO to sense complex precipitable structures, information that will be provided along with thermodynamic profiles and increase the applications of the RO technique.

Acknowledgements. This study has been conducted under the Spanish ACI2010-1089 and AYA2011-29183-C02-02 grant, with contributions from EUMETSAT's ROM SAF CDOP2 and two NASA ROSES. RP is under the Spanish FPI program and he also enjoyed two JPL Vistor Student Researcher Program invitations. EC is under the Spanish Ramon y Cajal programme. A relevant contribution to the logistics and implementation of the experimental site was done by Adriano Camps' group at the Remote Sensing Lab, department of Teoria del Senyal i Comunicacions, Universitat Politècnica de Catalunya, under grant AYA2011-29183-C02-01. Some of these grants are partially funded by the European ERDF/FEDER programme. Work performed at the Jet Propulsion Laboratory (JPL), California Institute of Technology, was supported under a contract with the National Aeronautics and Space Administration.

The Helmholtz-Centre German Research Centre for Geosciences (GFZ Potsdam) provided the JAVAD GPS receiver. Results obtained thanks to the meteorological data provided by the Servei Meteorològic de Catalunya (METEOCAT), the Agencia Estatal de Meteorología, Ministerio de Agricultura, Alimentación y Medio Ambiente (AEMET) and the European Organisation for the Exploitation of Meteorological Satellites (EUMETSAT). The experimental site belongs to the Spanish Ministry of Defense, Estado Mayor de la Defensa (EMAD).

Bruce T. Draine and Piotr J. Flatau are gratefully acknowledged for providing the DDscat code. Particle shapes for DDScat code were provided by Dr. G. Liu and Ryan ~~Honeyagen~~Honeyager, from Florida State University. The authors want to thank G. Hajj for interesting discussions about the ionosphere.

References

Aminou, D. M.: MSG's SEVIRI Instrument, ESA Bulletin, 111, 15–17, 2002.

Aparicio, J. M. and Rius, A.: A raytracing inversion procedure for the extraction of the atmospheric refractivity from GNSS travel-time data, Physics and Chemistry of the Earth, Parts A/B/C, 29, 213–224, doi:10.1016/j.pce.2004.01.008, http://linkinghub.elsevier.com/retrieve/pii/S1474706504000191, 2004.

Baldini, L. and Gorgucci, E.: Identification of the melting layer through dual-polarization radar measurements at vertical incidence, Journal of Atmospheric and Oceanic Technology, 23, 829–839, doi:10.1175/JTECH1884.1, 2006.

Beard, K. V. and Chuang, C.: A new model for the equilibrium shape of raindrops, Journal of the Atmospheric sciences, 44, 1509–1524, http://journals.ametsoc.org/doi/abs/10.1175/1520-0469(1987)044{%}3C1509:ANMFTE{%}3E2.0.CO;2, 1987.

Bech, J., Vilaclara, E., Pineda, N., Rigo, T., Lopez, J., O'Hora, F., Lorente, J., Sempere, D., and Fabregas, F. X.: The weather radar network of the Catalan Meteorological Service: description and applications, in: Proceedings of ERAD, vol. 2, pp. 416–420, 2004.

Black, R. A. and Hallett, J.: Rain Rate and Water Content in Hurricanes Compared with Summer Rain in Miami, Florida, Journal of Applied Meteorology and Climatology, 51, 2218–2235, doi:10.1175/JAMC-D-11-0144.1, http://journals.ametsoc.org/doi/abs/10.1175/JAMC-D-11-0144.1, 2012.

Blewitt, G.: Carrier phase ambiguity resolution for the Global Positioning System applied to geodetic baselines up to 2000 km, Journal of Geophysical Research, 94, 10 187–10 203, doi:10.1029/JB094iB08p10187, 1989.

Bringi, V. N. and Chandrasekar, V.: Polarimetric weather radar; principles and applications, Cambridge University Press, 2001.

Cardellach, E., Tomás, S., Oliveras, S., Padullés, R., Rius, A., de la Torre-Juárez, M., Turk, F. J., Ao, C. O., Kursinski, E. R., Schreiner, W., Ector, D., and Cucurull, L.: Sensitivity of PAZ LEO Polarimetric GNSS Radio-Occultation Experiment to Precipitation Events, IEEE Transactions on Geoscience and Remote Sensing, 53, 190–206, doi:10.1109/TGRS.2014.2320309, 2015.

Cucurull, L. and Derber, J. C.: Operational Implementation of COSMIC Observations into NCEP's Global Data Assimilation System, Weather and Forecasting, 23, 702–711, doi:10.1175/2008WAF2007070.1, http://journals.ametsoc.org/doi/abs/10.1175/2008WAF2007070.1, 2008.

Delanoë, J. and Hogan, R. J.: Combined CloudSat-CALIPSO-MODIS retrievals of the properties of ice clouds, Journal of Geophysical Research, 115, D00H29, doi:10.1029/2009JD012346, http://doi.wiley.com/10.1029/2009JD012346, 2010.

Draine, B. T. and Flatau, P. J.: Discrete-dipole approximation for scattering calculations, Journal of the Optical Society of America A, 11, 1491, doi:10.1364/JOSAA.11.001491, http://www.opticsinfobase.org/abstract.cfm?URI=josaa-11-4-1491, 1994.

Draine, B. T. and Flatau, P. J.: User Guide for the Discrete Dipole Approximation Code DDSCAT 7.3, arXiv preprint, 3, http://arxiv.org/abs/1305.6497, 2013.

Ducrocq, V., Braud, I., Davolio, S., Ferretti, R., Flamant, C., Jansa, A., Kalthoff, N., Richard, E., Taupier-Letage, I., Ayral, P. A., Belamari, S., Berne, A., Borga, M., Boudevillain, B., Bock, O., Boichard, J. L., Bouin, M. N., Bousquet, O., Bouvier, C., Chiggiato, J., Cimini, D., Corsmeier, U., Coppola, L., Cocquerez, P., Defer, E., Delanoë, J., Di Girolamo, P., Doerenbecher, A., Drobinski, P., Dufournet, Y., Fourrié, N., Gourley,

J. J., Labatut, L., Lambert, D., Le Coz, J., Marzano, F. S., Molinié, G., Montani, A., Nord, G., Nuret, M., Ramage, K., Rison, B., Roussot, O., Said, F., Schwarzenboeck, A., Testor, P., Van Baelen, J., Vincendon, B., Aran, M., and Tamayo, J.: HyMeX-SOP1, the field campaign dedicated to heavy precipitation and flash flooding in the northwestern Mediterranean, Bulletin of the American Meteorological Society, 95, 1083–1100, doi:10.1175/BAMS-D-12-00244.1, http://journals.ametsoc.org/doi/abs/10.1175/BAMS-D-12-00244.1?af=R, 2014.

Healy, S. B., Haase, J. S., and Lesne, O.: Abel transform inversion of radio occultation measurements made with a receiver inside the Earth's atmosphere, Annales Geophysicae, 20, 1253–1256, 2002.

Healy, S. B., Jupp, A. M., and Marquardt, C.: Forecast impact experiment with GPS radio occultation measurements, Geophysical Research Letters, 32, L03 804, doi:10.1029/2004GL020806, http://doi.wiley.com/10.1029/2004GL020806, 2005.

Kennedy, P. C. and Rutledge, S. A.: S-Band Dual-Polarization Radar Observations of Winter Storms, Journal of Applied Meteorology and Climatology, 50, 844–858, doi:10.1175/2010JAMC2558.1, http://journals.ametsoc.org/doi/abs/10.1175/2010JAMC2558.1, 2011.

Kursinski, E. R., Hajj, G. A., Schofield, J. T., Linfield, R. P., and Hardy, K. R.: Observing Earth's atmosphere with radio occultation measurements using the Global Positioning System, Journal of Geophysical Research, 102, 23 429–23 465, doi:10.1029/97JD01569, http://onlinelibrary.wiley.com/doi/10.1029/97JD01569/full, 1997.

Liu, G.: A Database of Microwave Single-Scattering Properties for Nonspherical Ice Particles, Bulletin of the American Meteorological Society, 89, 1563–1570, doi:10.1175/2008BAMS2486.1, http://journals.ametsoc.org/doi/abs/10.1175/2008BAMS2486.1, 2008.

Matrosov, S. Y.: Radar reflectivity in snowfall, IEEE Transactions on Geoscience and Remote Sensing, 30, 454–461, doi:10.1109/36.142923, 1992.

Matrosov, S. Y. and Mace, G. G.: Observations of ice crystal habits with a scanning polarimetric W-band radar at slant linear depolarization ratio mode, Journal of Atmospheric and Oceanic Technology, 29, 989–1008, doi:10.1175/JTECH-D-11-00131.1, http://journals.ametsoc.org/doi/abs/10.1175/JTECH-D-11-00131.1, 2012.

Noel, V. and Chepfer, H.: A global view of horizontally oriented crystals in ice clouds from Cloud-Aerosol Lidar and Infrared Pathfinder Satellite Observation (CALIPSO), Journal of Geophysical Research, 115, doi:10.1029/2009JD012365, http://doi.wiley.com/10.1029/2009JD012365, 2010.

Rocken, C., Anthes, R. A., Exner, M., Hunt, D., Sokolovskiy, R., Ware, R. H., Gorbunov, M., Schreiner, W., Feng, D., Herman, B. M., Kuo, Y. H., and Zou, X.: Analysis and validation of GPS/MET data in the neutral atmosphere, Journal of Geophysical Research, 102, 29,849–29,866, doi:10.1029/97JD02400, http://onlinelibrary.wiley.com/doi/10.1029/97JD02400/full, 1997.

Ryzhkov, A. V. and Zrnić, D. S.: Polarimetric method for ice water content determination, Journal of Applied meteorology, 37, 125–134, http://ieeexplore.ieee.org/xpls/abs{_}all.jsp?arnumber=516402, 1998.

Smith, P. L.: Equivalent Radar Reflectivity Factors for Snow and Ice Particles, Journal of Climate and Applied Meteorology, 23, 1258–1260, doi:10.1175/1520-0450(1984)023<1258:ERRFFS>2.0.CO;2, 1984.

Steiner, A. K., Lackner, B. C., Ladstdter, F., Scherllin-Pirscher, B., Foelsche, U., and Kirchengast, G.: GPS radio occultation for climate monitoring and change detection, Radio Science, 46, 1–17, doi:10.1029/2010RS004614, 2011.

Trömel, S., Kumjian, M. R., Ryzhkov, A. V., Simmer, C., and Diederich, M.: Backscatter differential phase-estimation and variability, Journal of Applied Meteorology and Climatology, 52, 2529–2548, doi:10.1175/JAMC-D-13-0124.1, 2013.

Ulbrich, C. W.: Natural Variations in the Analytical Form of the Raindrop Size Distribution, Journal of Climate and Applied Meteorology, 22, 1764–1775, doi:10.1175/1520-0450(1983)022<1764:NVITAF>2.0.CO;2, 1983.

Vivekanandan, J., Bringi, V. N., Hagen, M., and Meischner, P.: Polarimetric radar studies of atmospheric ice particles, IEEE Transactions on Geoscience and Remote Sensing, 32, 1–10, doi:10.1109/36.285183, http://ieeexplore.ieee.org/lpdocs/epic03/wrapper.htm?arnumber=285183, 1994.

Walpole, R. E., Myers, R. H., Myers, S. L., and Ye, K.: Probability and Statistics for Engineers and Scientists, Prentice Hall, Boston, 9th edn., 2012.

Williams, C. R., Bringi, V. N., Carey, L. D., Chandrasekar, V., Gatlin, P. N., Haddad, Z. S., Meneghini, R., Joseph M., S., Nesbitt, S. W., Petersen, W. A., Tanelli, S., Tokay, A., Wilson, A., and Wolff, D. B.: Describing the Shape of Raindrop Size Distributions Using Uncorrelated Raindrop Mass Spectrum Parameters, Journal of Applied Meteorology and Climatology, 53, 1282–1296, doi:10.1175/JAMC-D-13-076.1, http://journals.ametsoc.org/doi/abs/10.1175/JAMC-D-13-076.1, 2014.

Yeh, K. C., Chao, H. Y., and Lin, K. H.: A study of the generalized Faraday effect in several media, Radio Science, 34, 139–153, doi:10.1029/98RS02442, http://doi.wiley.com/10.1029/98RS02442, 1999.

Zhang, J., Crocker, N. A., Carter, T. A., Kubota, S., and Peebles, W. A.: Interaction between Faraday rotation and Cotton-Mouton effects in polarimetry modeling for NSTX, Review of Scientific Instruments, 81, 3–6, doi:10.1063/1.3479042, 2010.

Table 1. Summary of the relevant differences expected between the ROHP-PAZ spaceborne experiment and the conducted ground-based field campaign.

Parameter	Ground-based experiment	ROHP-PAZ
phase delay	unknown, need to subtract the mean value of each measured arc (Eq. 4)	calibrated from the polarimetric phase difference at highest layers of the atmosphere
Local multipath	multiple reflectors and environmental dependency because of dry/wet changes in electrical permittivity of soil and structures	expected stable properties of local satellite structure. No expected dependency on the environment
Thermodynamic profiles	refractivity, pressure, temperature and humidity cannot be extracted	refractivity, pressure, temperature and humidity can be derived

Table 2. Summary of the standard deviation analysis ~~, using~~ for the polarimetric phase differences under three different ~~day sets~~meteorological conditions (dry, wet and rain days). $\overline{\sigma_i}$ and N_i account for the mean standard deviation and the number of used days for each ~~day set~~ meteorological condition group i. P_F is the cumulative probability associated to the f statistic comparing the σ of the rain and the no-rain (wet and dry) days. The f statistic is the result of the F-test and P_F can be understood as the significance level at which we are rejecting the null hypothesis that both populations come from the same pool.

PRN	$\overline{\sigma_{dry}}$ (mm)	N_{dry}	$\overline{\sigma_{wet}}$ (mm)	N_{wet}	$\overline{\sigma_{rain}}$ (mm)	N_{rain}	P_F
G10	2.706	20	2.895	112	3.992	25	0.99
G15	1.808	20	2.263	108	2.597	29	0.89
G22	2.565	20	3.167	113	3.738	24	0.91
~~G26~~ G14	3.386	20	3.698	114	4.108	23	0.79
G31	1.809	20	1.876	113	2.584	24	0.99

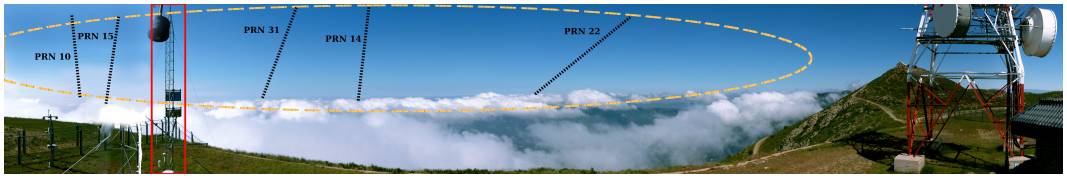

Figure 1. Panoramic view from the observation site. The field of view is the area compressing azimuths from $\sim 160^\circ$ (left) to $\sim 270^\circ$ (right), looking south. The yellow long-dashed line indicates the main lobe of the antenna (approximate). The black dashed lines represent the tracks of the followed GPS satellites: from left to right, PRN 10, 15, 31, 14 and 22. Multiple metallic elements seen in the field of view, such as the meteorological station (inside the red solid line square), the fence, the telecommunications antenna, etc. and others not pictured (metallic shelter, antenna supports...) could affect the GNSS signal in the form of multipath.

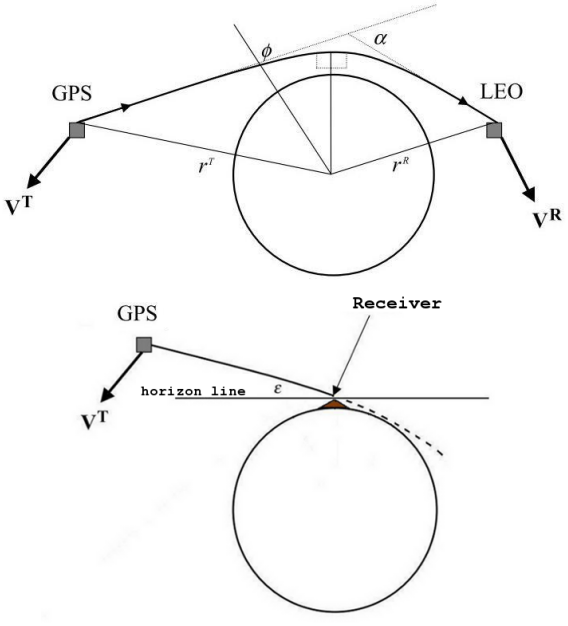

Figure 2. (top) Standard radio occultation geometry. (bottom) GPS-receiver radio link in a on ground receiver geometry, such as the one used in this experiment. ϵ accounts for elevation. Edited figure from original in Healy et al. (2002).

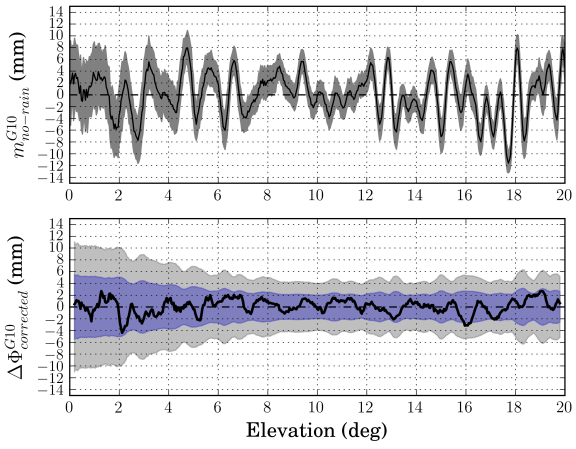

Figure 3. Examples of (top) local multipath pattern after Eq. 4 for PRN 10 ($m^{G10}_{no-rain}, \sigma^{G10}_{no-rain}$), using a total of 132 days defined as *no-rain* days. Notice the large standard deviation at lower elevations, and $\sigma^{G10}_{no-rain}$ of about 2 mm at higher elevations. (bottom) Corrected $\Delta\Phi^{PRN}_{day}(\epsilon)$ for 2014/04/16 (black line) after applying Eq. 5. The 1- and 2-σ thresholds (local multipath standard deviation) are represented in blue and gray, respectively.

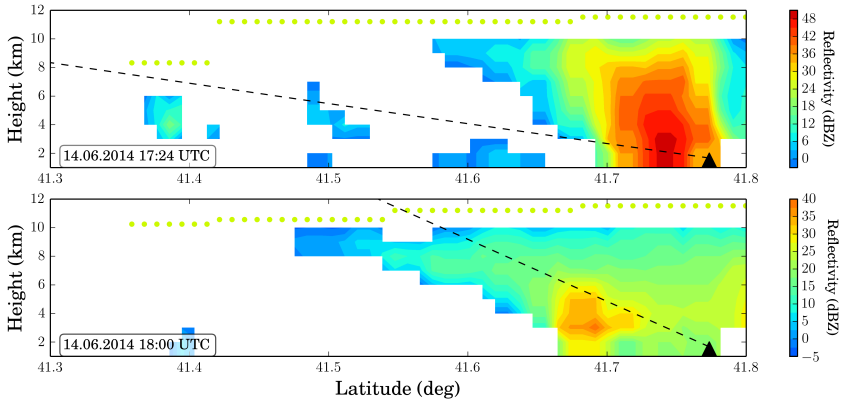

Figure 4. ~~Illustration of the performed collocation at two different times of the same observation, a rising satellite link.~~ A vertical slice of ~~the~~ radar reflectivity ~~has been collocated with the Cloud top Phase (CP~~shaded) ~~product and the ray trajectory~~at two epochs of a rising GNSS occultation event. The dashed black line is the projection of the ray trajectory as simulated with OAT ray tracer on the described plane, and the dots correspond to the Cloud top Phase (CP) products. In this case, all the green dots indicate ice in the top of the clouds.

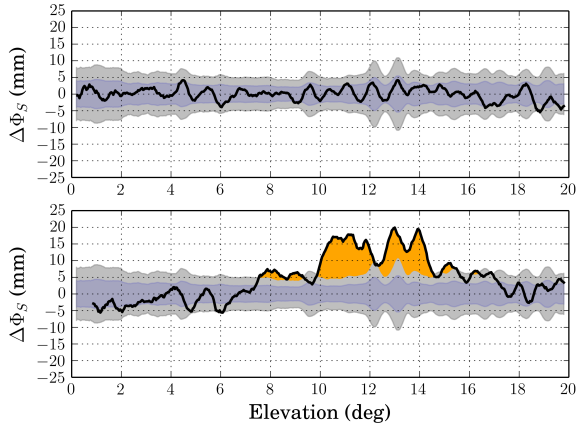

Figure 5. Examples of $\Delta\Phi_S(\epsilon)$ (black line), the $\pm\sigma_{no-rain}$ contour (blue) and the $\pm 2\sigma_{no-rain}$ contour (gray), for two observations of the PRN G22 during 2014/05/26 (top) and 2014/06/14 (bottom). The top $\Delta\Phi_S(\epsilon)$ measurement is well inside the 2 σ contour, showing no polarimetric signatures. On the bottom, case on 2014/06/14 shows large positive $\Delta\Phi_S(\epsilon)$. The value of $\Delta\Phi_S(\epsilon)$ above $2\sigma_{no-rain}$ threshold will be called hereafter $\Delta\Phi_+$, and its area (orange zone) A_Φ.

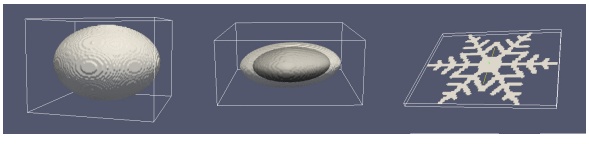

Figure 6. ~~Target shapes~~ Particle shape models used in DDScat. (left) Oblate ellipsoid ~~, used to reproduce~~ for rain drops~~.~~, (middle) ~~Two~~ two concentric ellipsoids ~~, used to simulated~~ for melting ice particles, with an ice core and a water shell~~.~~, (right) ~~Dendritic~~ dendritic shape ~~used to simulate the~~ for1 pristine ice particles.

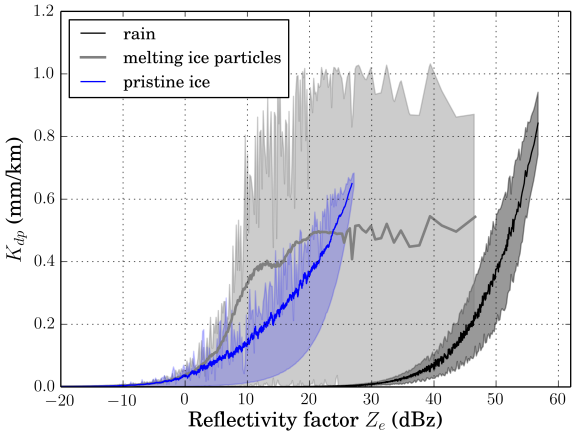

Figure 7. $K_{dp}(Z_e)$ for all the possible physically valid $N(D)$ for each ~~hydrometheor~~ hydrometeor type: rain (black), melting ice particles (gray) and ice crystals (blue). Rain drops need high reflectivity to produce high K_{dp}, while ice crystals and melting ice particles can induce high values of K_{dp} at smaller values of Z_e. The thick lines overplotted represent the Z_e - K_{dp} relation used in this analysis for each hydrometeor type.

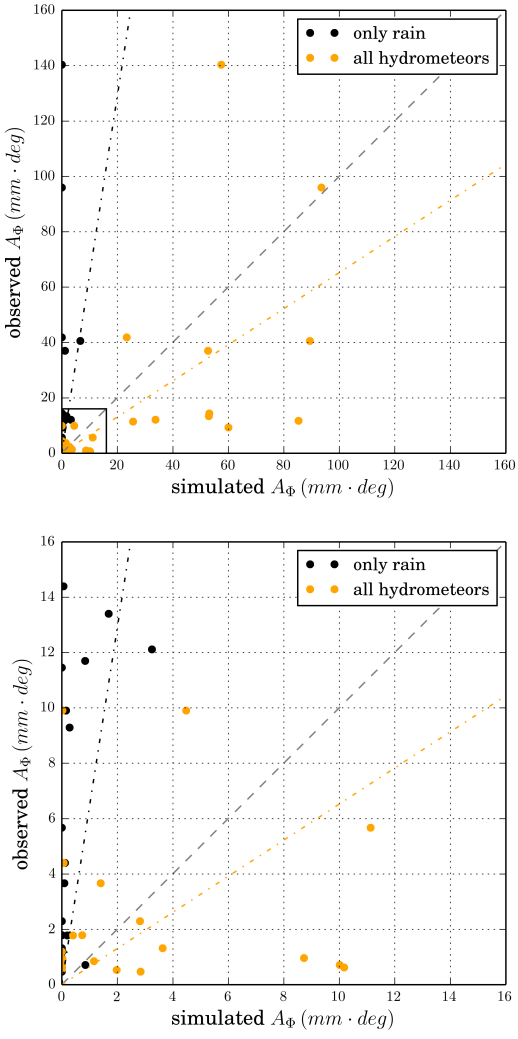

Figure 8. (top) Observed versus simulated A_Φ. ~~A *zoom* of the lowest region in the~~ (bottom~~panel~~) In more detail, the area where $A_\Phi < 20$ mm·deg. Black dots represent the simulated A_Φ using only rain drops, while orange dots represent the simulated A_Φ accounting for ice crystals and melting ice particles too. The ~~gray dashed~~ dash-dot lines represent the best fitted line ~~represents~~ to the ~~perfect agreement between the observations only rain~~ A_Φ (black) and to the ~~modelling. The correlation coefficients for the data is $r = 0.60$~~rain, ice and ~~it decreases to $r = 0.75$ when we take into account only the points with an observed $A_\Phi < 20$ mm·deg~~melting particles A_Φ (orange).

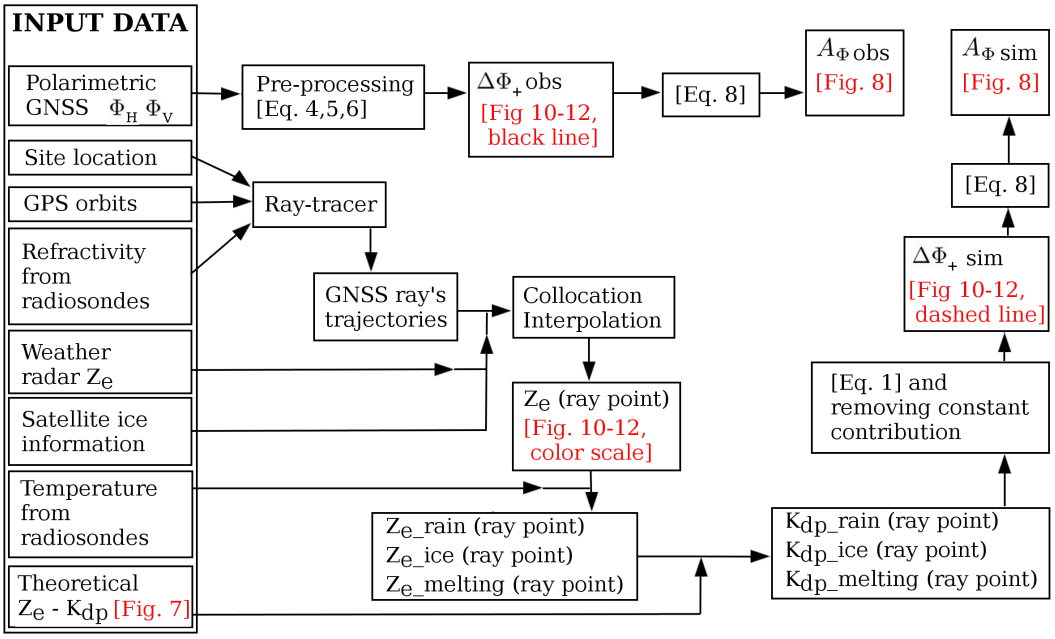

Figure 9. Block diagram showing all the data analysis and modelling process. Steps from the data aquisition to the final results are shown.

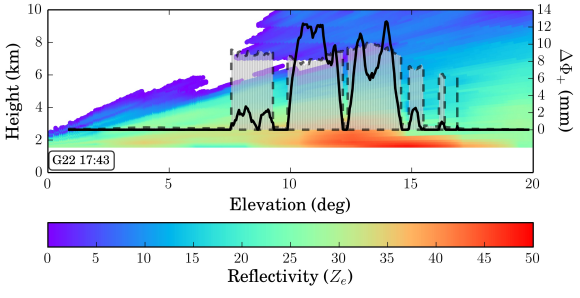

Figure 10. Each GNSS ray is identified by its elevation angle. Along a ray, each point can be identified by its height. The color scale shows the weather radar reflectivity Z_e interpolated along the GNSS rays. The black line is the observed $\Delta\Phi_+$ (right Y axis). Simulation results performed as described in Sect. 5 are represented ~~in orange shaded areas~~with dashed lines. In the regions where actual data showed $\Delta\Phi_+ > 0$, all hydrometeors are taken into account in the simulations. Only rain is simulated otherwise. Note also that fully oriented ice crystals have been considered in the simulation (it might not be necessary the case, information not available).

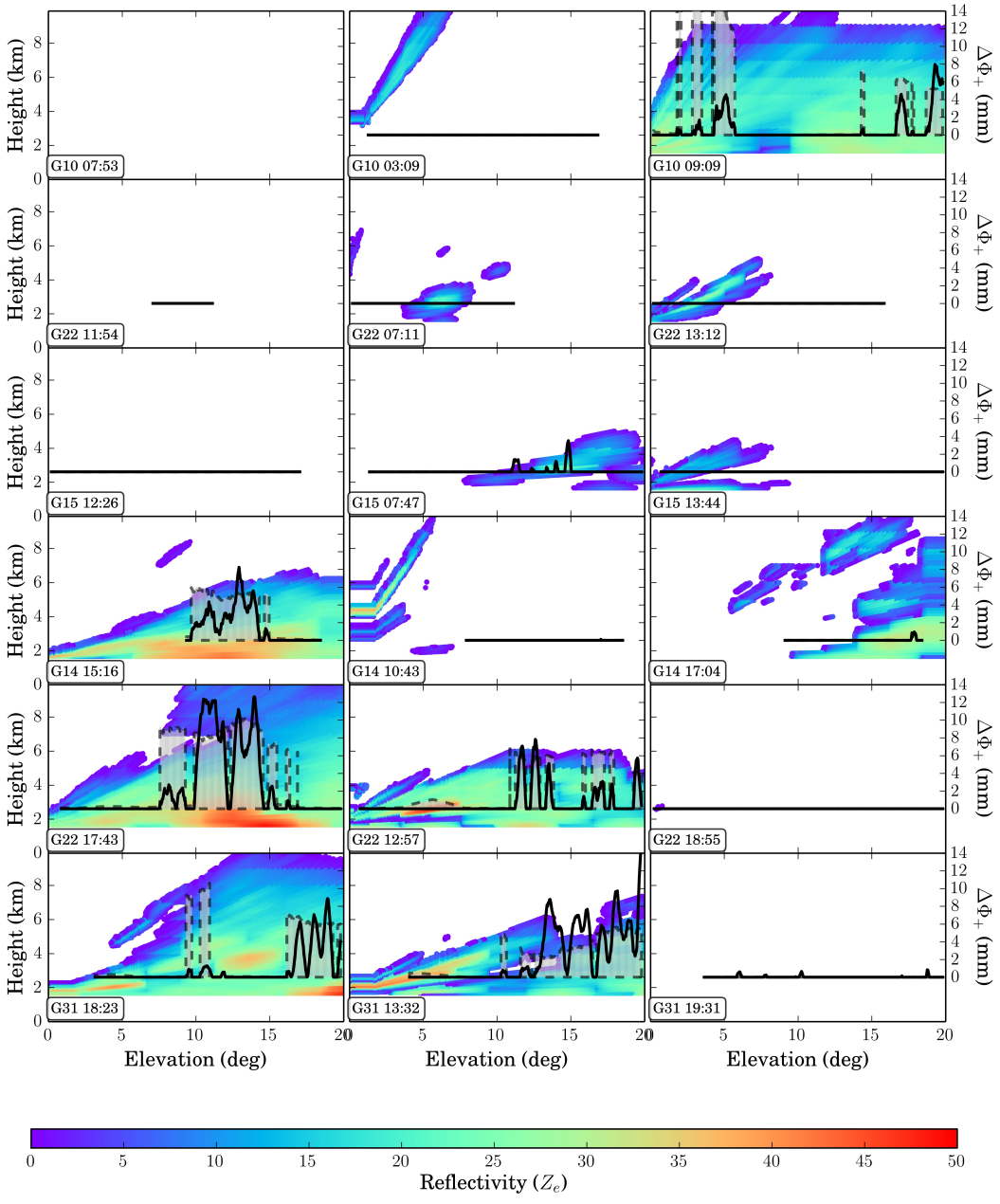

Figure 11. Rain episodes on 2014/06/14 (left), 2014/08/22 (middle) and 2014/05/26 (right). Each panel corresponds to a PRN, identified in the label on the lower left corner, along with the time ~~of~~ when the ~~observation start~~satellite is at 10 deg. of elevation. Note that the radio-link with different PRNs corresponds to different time and also different azimuth. They are sorted in time, with the first one on the top. Content of each panel is explained in Fig. 10 caption.

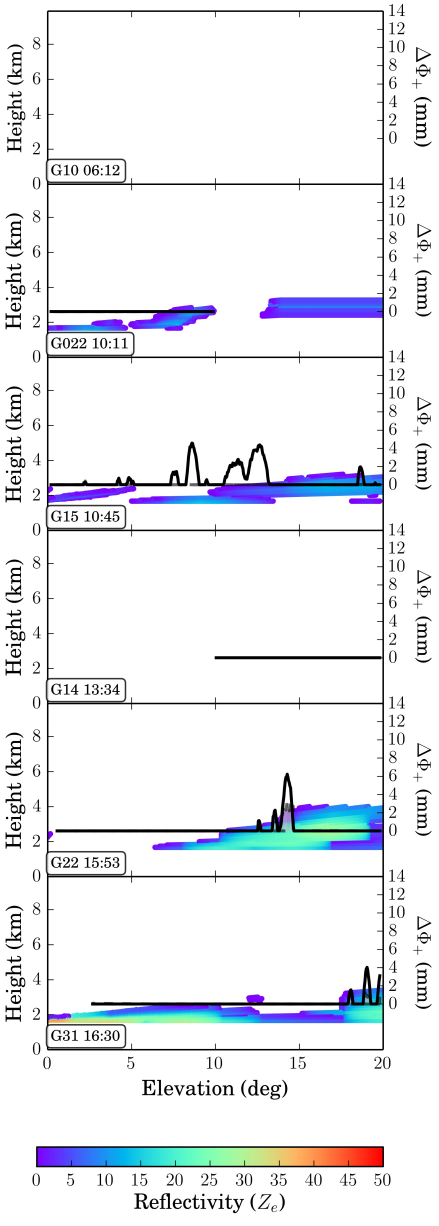

Figure 12. Same as Fig.11, but for 2014/07/09. The signal in PRN G15 could not be explained with the ~~used hydrometeors~~model simulation.